Online Research @ Cardiff

This is an Open Access document downloaded from ORCA, Cardiff University's institutional repository: https://orca.cardiff.ac.uk/id/eprint/130109/

This is the author's version of a work that was submitted to / accepted for publication.

Citation for final published version:

Lloyd, David ORCID: https://orcid.org/0000-0002-5656-0571, Millet, Coralie O., Williams, Catrin F. ORCID: https://orcid.org/0000-0001-8619-2581, Hayes, Anthony, Pope, Simon J. A. ORCID: https://orcid.org/0000-0001-9110-9711, Pope, Iestyn, Borri, Paola ORCID: https://orcid.org/0000-0002-7873-3314, Langbein, Wolfgang ORCID: https://orcid.org/0000-0001-9786-1023, Olsen, Lars Folke, Isaacs, Marc and Lunding, Anita 2020. Functional imaging of a model unicell: Spironucleus vortens as an anaerobic but aerotolerant flagellated protist. Advances in Microbial Physiology 76 , pp. 41-79. 10.1016/bs.ampbs.2020.01.002 file

Publishers page: http://doi.org/10.1016/bs.ampbs.2020.01.002 <http://doi.org/10.1016/bs.ampbs.2020.01.002>

Please note:
Changes made as a result of publishing processes such as copy-editing, formatting and page numbers may not be reflected in this version. For the definitive version of this publication, please refer to the published source. You are advised to consult the publisher's version if you wish to cite this paper.

This version is being made available in accordance with publisher policies. See http://orca.cf.ac.uk/policies.html for usage policies. Copyright and moral rights for publications made available in ORCA are retained by the copyright holders.

information services
gwasanaethau gwybodaeth

Running Title: Functional Imaging of a Model Unicell

CHAPTER

Functional imaging of a model unicell: *Spironucleus vortens* as an anaerobic but aerotolerant flagellated protist

David Lloyd[a, b]*, Coralie O. Millet[a], Catrin F. Williams[b], Anthony J. Hayes[a], Simon J.A. Pope[c], Iestyn Pope [a], Paola Borri[a], Wolfgang Langbein [d], Lars Folke Olsen[e], Marc D. Isaacs [a] and Anita Lunding[e]

[a]School of Biosciences, Cardiff University, Sir Martin Evans Building, Museum Avenue, Cathays Park, Cardiff CF10 3AX, Wales, UK
[b]School of Engineering, Cardiff Queen's Buildings, Newport Road, Cardiff CF24 3AA, Wales, UK
[c]School of Chemistry, Main Building, Cardiff University, Cardiff CF10 3AT, Wales, UK
[d]School of Physics and Astronomy, Cardiff University, The Parade, Cardiff CF24 3AA, Wales, UK
[e]Biochemistry and Molecular Biology, University of Southern Denmark, Campusvej 55, DK5230, Odense M, Denmark
*Corresponding author: E-mail: lloydd@cardiff.ac.uk

Abbreviations

CARS	Coherent anti-Stokes Raman scattering
CTC	5-cyano-2, 3-di-(*p*-tolyl) tetrazolium Cl
DAPI	4'-6-Diamino-2-phenylindole
FLIM	Fluorescence Lifetime Imaging Microscopy
TPF	Two Photon Fluorescence
SHG	Second Harmonic Generation
ILCT	Inter Ligand Charge Transfer
MLCT	Metal Ligand Charge Transfer

David Lloyd	lloydd@cardiff.ac.uk	(1,2)
Coralie O Millet	milletco@googlemail.com	(1)
Catrin F Williams	williamscf@cardiff.ac.uk	(2)
Anthony J Hayes	hayesaj@cardiff.ac.uk	(1)
Simon J A Pope	popesj@cardiff.ac.uk	(3)
Iestyn Pope	popei@cardiff.ac.uk	(1)
Paola Borri	borrip@cardiff.ac.uk	(1)
Wolfgang Langbein	langbeinww@cardiff.ac.uk	(4)
Lars Folke Olsen	lfo@bmb.sdu.dk	(5)
Marc D Isaacs	isaacsmd@cardiff.ac.uk	(1)
Anita Lunding	lunding@bmb.sdu.dk	(5)

Contents

5. Discussion

Abstract

Advances in optical microscopy are continually narrowing the chasm in our appreciation of biological organisation between the molecular and cellular levels, but many practical problems are still limiting. Observation is always limited by the rapid dynamics of ultrastructural modifications of intracellular components, and often by cell motility: imaging of the unicellular protist parasite of ornamental fish, *Spironucleus vortens*, has proved challenging. Autofluorescence of nicotinamide nucleotides and flavins in the 400-580 nm region of the visible spectrum, is the most useful indicator of cellular redox state and hence vitality. Fluorophores emitting in the red or near- infrared (i.e., phosphors) are less damaging and more penetrative than many routinely employed fluors. Mountants containing free radical scavengers minimise fluorophore photobleaching. Two-photon excitation provides a small focal spot, increased penetration, minimises photon scattering and enables extended observations. Use of quantum dots clarifies the competition between endosomal uptake and exosomal extrusion. Rapid motility (161µm/s) of the organism makes high resolution of ultrastructure difficult even at high scan speeds. Use of voltage-sensitive dyes determining transmembrane potentials of plasma membrane and hydrogenosomes (modified mitochondria) is also hindered by intracellular motion and controlled anaesthesia perturbs membrane organisation. Specificity of luminophore binding is always questionable; e.g. cationic lipophilic species widely used to measure membrane potentials also enter membrane-bounded neutral lipid droplet-filled organelles. This appears to be the case in *S. vortens*, where Coherent Anti-Stokes Raman Scattering (CARS) micro-spectroscopy unequivocally images the latter and simultaneous provides spectral identification at 2840cm^{-1}. Secondary Harmonic Generation highlights the highly ordered structure of the flagella.

Keywords

Fluorescence microscopy; Two photon excitation; Redox state; Photobleaching, Nuclei; Hydrogenosomes; Lipid droplets; Flagella;

Coherent Anti-Stokes Raman Scattering micro-spectroscopy; Second Harmonic Generation

1.Fluorescence and Phosphorescence

1.1 Fluorescence

Rapid advances in understanding of microbial structure and function rely on the development of novel fluorescence techniques and the implementation of new fluorescent probes. Whereas conventional optical methods are diffraction limited to 200nm spatial resolution for photons in the visible spectrum and only marginally better by UV-microscopy, new 'super-resolution' modifications permit a 20-100 nm range of observation. Fluorescence imaging has greatly extended understanding of cellular ultrastructure and dynamics, and advances in applications to fundamental biophysical problems and molecular biology proceed apace.

The absorption of light and its emission by molecules as fluorescence or phosphorescence may be represented as an energy diagram (Fig. 1). Absorption of photons occurs by transitions from the singlet ground state S_0, to the first and second singlet electronic states S_1 and S_2. This is followed, in the case of a fluorescence-emitting molecule, by fast (~10^{-15} s) internal conversion (thermal equilibration). This time interval is too short for significant movement of nuclei (the Franck-Condon principle). Emission then occurs from this fluorescent state by a return to the ground state.

In a phosphorescent molecule inter-system crossover into a forbidden, and hence long-lived, triplet state precedes emission.

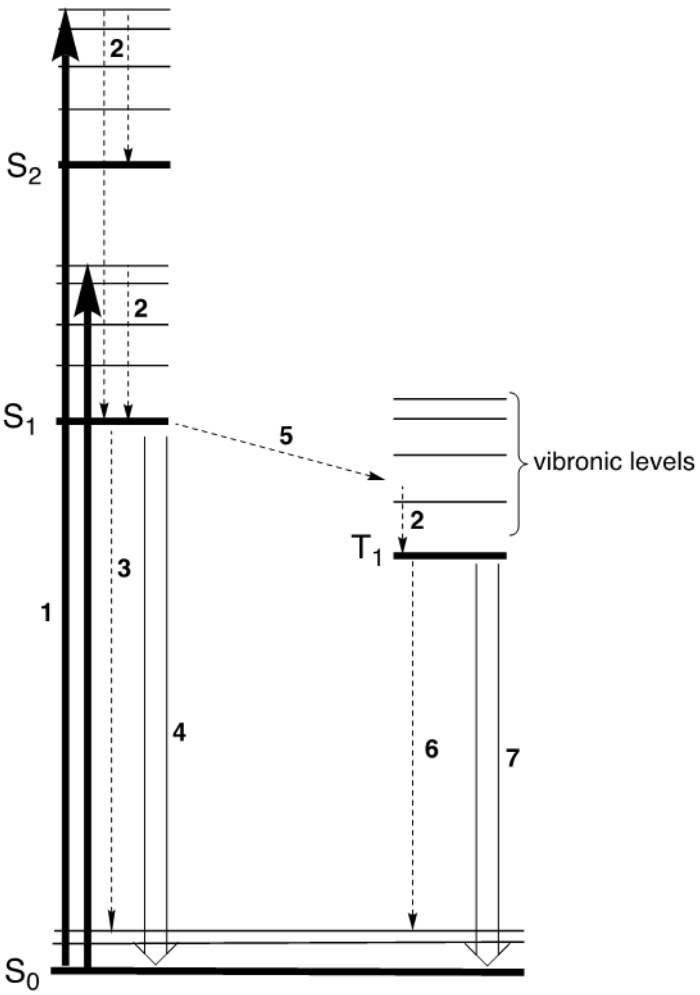

Fig. 1. Jablonski diagram for transitions involved in fluorescence and Phosphorescence. 1. Absorption of photons / energy. 2. Internal conversion. 3. Non-radiative deactivation of S_1. 4. Fluorescence emission. 5. Intersystem crossing (S_1 ➔ T_1). 6. Non-radiative deactivation of T_1. 7. Phosphorescence emission.

The basic principles of the absorption and emission of radiation are:

a. Only radiations that are absorbed by a radiating system are effective in producing chemical change (the Grotthuss-Draper law).

b. Only photons that are absorbed may give rise to emitted fluorescence.

c. The quantum efficiency is the ratio of quanta emitted as fluorescence to the quanta absorbed.

d. The maximum electronic transition probability is into the excited level corresponding to the maximum of the absorption band.

e. Therefore the fluorescence excitation spectrum is almost always identical to the absorption spectrum.

f. The fluorescence emission spectrum is independent of the exciting wavelength.

g. The fluorescence emission spectrum can be a 'mirror image' of the lowest energy absorption band.

h. The maximum of emission is at a longer wavelength than the observed absorption maximum (Stokes' Law).

i. Lifetimes of emitted luminescence for fluorescence are typically measured as low values of <50ns and those for phosphorescence range from µsec to many msec.

The properties of compounds useful for imaging applications include:

a. Ease of penetration of the cell wall, cytoplasmic and organelle membranes (dependent on lipophilicity, size and charge).
b. Persistence (resistance to photobleaching, loss on washing of cells, or active extrusion). DABCO (1, 4-diazobicyclo [2. 2. 2.] octane) a quencher of singlet oxygen, protects against free-radicals and acts as an 'antifade' agent. Otherwise 'Vectashield' mounting medium is commonly used.
c. Uniform distribution in the solvent, without aggregation, or precipitation.
d. Well-defined and efficient characteristics of photon absorption and emission (i.e., high values of absorption coefficients and favourable quantum yields) within the ambient intracellular pH and ionic composition of the cytosol and subsequent to binding to membranes and organelles.

e. Minimal invasive effects on metabolic processes over short exposure times.
f. Minimal toxicity as measured by vitality (e.g., intracellular or whole cell motility) or viability (growth and reproduction).

1.2 Phosphorescence

Many phosphorescent luminophores offer superior properties to those of fluorescent probes (Coogan et al., 2010, Lloyd et al., 2012): these include:

a. Broad peaks of emission thoughout the visible and near IR.
b. Long luminescence lifetimes tenths of µsec to milliseconds.
c. Luminescence quantum yields in excess of 0.5.
d. Large Stokes shifts: often exceeding 5,000cm^{-1}.
e. Favourable chemical, photochemical, thermal and metabolic stabilities.

2.Spironucleus vortens: the organism

Spironucleus vortens is an aerotolerant microaerophilic protozoan inhabitant of ornamental fish, most often symbiotically occurring in the intestinal tract of healthy fish (Poynton & Morrison, 1990, Poynton et al., 1995, 2004). Under stressful environmental circumstances (Lloyd and Williams, 1993), *e.g*., elevated temperatures, or low dissolved O_2, (Lloyd et al., 1993,Lloyd 2002; Lloyd and Williams, 2015), this organism becomes parasitic, causing a systemic infection leading to host pathophysiology, morbidity and mortality. These symptoms are associated with skin lesions and probably 'hole-in-the-head' disease in cichlids (Paull & Matthews, 2001).

Other related species (Sterud, 1998, Sterud and Poynton, 1998) are of worldwide distribution, and although also of great economic importance still not completely defined taxonomically (Fard et al., 2007; Denikina et al., 2016, 2018, 2019). *S. barkhanus* (Sterud et al., 1997, 1998), is a non-pathogenic commensal, whereas *S.*

salmonicida is a highly infectious species (Jørgensen & Sterud, 2006, Roxström-Lindquist et al., 2014, Jørgensen et al., 2011), causing huge economic losses in wild and farmed food fish (trout and salmon). The pathogenicity of this latter species appears to be potentiated by O_2, as it has been shown that this inducer up-regulates a host of enzymes enabling the spread of organisms from the gut to peripheral (and more aerobic) tissues of the fish (Stairs et al., 2019). Also infected are crustaceans and shellfish in cold, temperate and tropical regions, as well as amphibians (*S. elegans*, Brugerolle et al., 1980). Other hexamitids are often free-living (Biagini et al., 1997b), or infect mammals, birds and reptiles (Brugerolle et al., 1980, Williams et al., 2011).

Uncovering the sub-cellular structure, physiology and biochemistry of *S. vortens* as a model organism will allow a better understanding of complex intracellular organisation, and may help lead to identification of potential therapeutic agents for prevention, treatment and limitation of the spread of infection.

S. vortens has 6 anterior locomotory flagella, one and a half times the body length, plus two longer posteria trailing ones, twice the body length. Restriction of the forward propulsive motility (steered mainly by the posteria flagella) can be reversibly achieved by 280mM chloral hydrate (2,2,2-trichloroethane-1,1-diol); recovery on washing away this anaesthetic takes about 20min. Otherwise aqueous methyl cellulose (10% w/v) or a thixotropic gel (Lloyd et al., 2015) is useful to diminish swimming speeds.

S. vortens, and *S. salmonicida* have both been shown to have hydrogenosomes (Millet et al., 2013; Jerlström-Hultqvist et al., 2013). In this respect they resemble many other microaerophilic protists inhabiting low O_2 environments. Thus those free-living in anaerobic sediments (Biagini et al.,1997 b), and also as symbiotic partners (Yarlett et al., 1981; Ellis et al., 1991; Millet et al., 2010a; Lantsman et al., 2008) or parasitic species of intestinal or urinogenital tracts (Lindmark and Muller, 1973; Paul et al., 1990), have hydrogenosomes. These mitochondrial-derived organelles (Horner et al., 1996; Biagini et al., 1997a) are autofluorescent redox-active organelles (Millet et al., 2013): they have flavin and iron-sulphur-based electron transport chains (Chapman et al., 1986b, Cammack et al. 2003). They are devoid of cytochromes and the energy transducing mechanisms characteristic of their evolutionary

precursors. Instead they have unusual bacterial-like (Biagini et al., 2003, Yarlett et al., 1994) enzymatic components (e.g. hydrogenase and pyruvate ferredoxin reductase). In *Giardia intestinalis*, mitosomes serve instead of hydrogenosomes, as even further evolutionary diminished mitochondria derived organelles (Lloyd et al., 2002; Tovar et al., 2003;). These features, alongside their O_2 scavenging mechanisms, provide useful growth inhibitory targets (e.g., by 5'nitroimidazoles, Williams et al., 2012a, and garlic-derived compounds, Millet et al., 2010b, Williams et al., 2014; Leitsch et al., 2018). Phagocytosis of quantum dots by *S. vortens* provides a glimpse into the process of uptake and subcellular organisation by the organism: however, it is important to differentiate these endocytotic vesicles, some of which appear similar in size to hydrogenosomes.

3. Live cell imaging

3.1 Autofluorescence

Reduced nicotinamide adenine dinucleotide (NADH) is the 'bellwether' of redox states of microorganisms as well as of the cells of higher organisms they infect (Chance et al., 1966), and is thus a key indicator of the vitality of health as well as a widely used diagnostic of nutrient deprivation ('starvation'), O_2 deprivation, oxidative stress, vitality, or viability of microbial single organisms or populations. Excitation of fluorescence of the reduced coenzyme at 366 ± 20 nm is optimal, and blue-green emission occurs at 450 ± 30 nm. When combined with measurements of oxidized flavoproteins (and including flavin adenine dinucleotide, i.e., FAD) (λ_{ex} 460 ± 5nm, λ_{em} 520 ± 20nm), and then calibrating with known standards, a redox index may be calculated using concentration based redox ratios:

Fp/(Fp +NADH) and NADH/Fp+NADH

These ratios have burgeoning applications in human physiological assessments, biomedical diagnoses and treatments (Li, et al., 2009, Xu et al., 2013).

In *S. vortens* the hydrogenosomes are the most prominent sites of autofluorescence due to oxidized flavin emission (Fig. 2). The emission intensities of both the reduced nicotinamide and oxidized flavin coenzymes oscillate with a period of about 50 min in washed whole-cell suspensions stirred under a gas phase of air (C. F. Williams and M. A. Aon, unpublished; Williams, 2013). The cytosol also provides a widely distributed diffuse background with a broad emission at between 470nm and 683nm (Fig. 2: Millet, 2010; Millet et al., 2013).

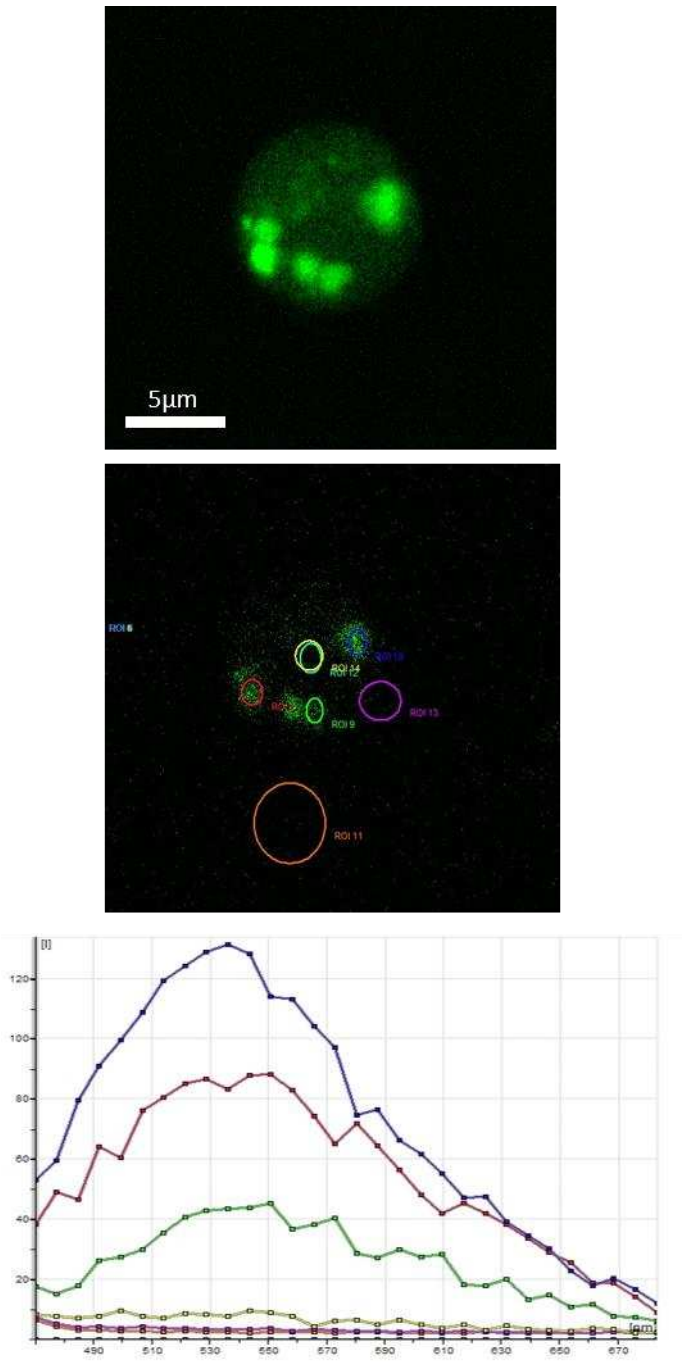

Fig. 2.Comparison of the autofluorescence spectra (λ_{ex} 458nm) of bright spherical inclusions in *S. vortens* (Regions Of Interest 1, 2, and 3) (and background areas within the cytosol, (ROIs 4 and 5), and extracellular medium (ROI 6). Ordinate: fluorescence emission intensity arbitrary units; abscissa: wavelength 470-683nm. Lambda scans were performed at 10nm intervals. Leica TCS SP2 AOBS Confocal Microscope, X100 objective, using

a 458nm Ar Ion laser line at 61% output intensity (Millet, 2010; Millet et al., 2013).

.

3.2 Quantum dot endocytosis and exocytosis

Phagocytosis of streptavidin-coated 15nm diam. cadmium selenide quantum dots (50ng/ml) by *S. vortens* provides images (λ_{ex} 405 ± 5nm, λ_{em}585 ± 20nm) of the processes of active uptake, aggregation into larger clusters, and extrusion of particles by the organism (Fig. 3) (Millet, 2010).
Initial uptake occurs within 2 s of incubation and is restricted to the region of flagellar pockets. Flow cytometry provided quantitative confirmation of the kinetics of these processes. Not all intestinal diplomonads have this capacity (Millet et al., 2011, Lloyd and Williams. 2014); thus for instance *Giardia intestinalis*, a parasite of the human upper intestine, can only perform pinocytosis for uptake of soluble compounds, relying on the host to supply pre-digested nutrients (Lloyd and Harris, 2002; Lloyd and Williams, 2014). In *S. vortens,* distribution to numerous peripherally situated small vacuoles then occurs, followed by concentration in larger vacuoles before extrusion over a period of 20 min. Ingestion of larger particles; e.g. fluorescent beads (~1µm diameter), or live rod-shaped bacteria (0.2 x 3 µm), did not occur. Transient labelling of larger endocytotic vesicles by quantum dots enables differentiation from the similarly-sized lipid droplets and hydrogenosomes.

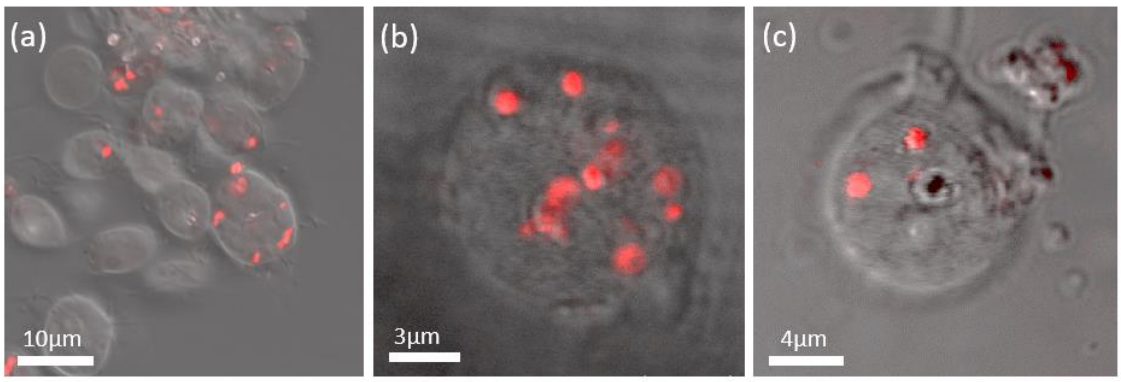

Fig. 3. Sampling after presentation of quantum dots to *S. vortens* after (a) 2 s, (b) 10 min and (c) 20 min of endocytosis/exocytosis. Each sample was fixed in 3% (v/v) formaldehyde solution immediately on collection (Millet, 2010). Individual and clusters (tiny, very bright) quantum dots can just be discerned especially in (a).

3.3 Routinely employed fluorophores

Diplomonad genera are characterised by the presence of paired nuclei, and in *Spironucleus* spp. these are close to the anterior pole of the spherical to pyriform (10-20 μm x 5-10 μm) organisms. DAPI (4'-6-diamino-2-phenylindole) (Fig. 4a), or Hoechst 33342 are the fluorophores of choice for live cell imaging of nuclei, the latter being less toxic.

Optical imaging of organelles in *S. vortens* has been problematic due to issues with the rapid swimming motility of the organism, and intracellular cytoplasmic organelle motion (cyclosis). Also several types of sub-cellular components are of similar sizes to hydrogenosomes (500 nm to1 μm diameter) (Fig.4b-e).

Also the specificity of luminophore binding is often questionable; thus many cationic lipophilic species (e.g., the carbocyanine probe, $DioC_6(3)$; Lloyd et al., 1996, 2018), Mito Tracker Green, or rhodamine 123(Millet, 2010), widely used to measure mitochondrial transmembrane electrochemical potentials, also bind to the lipoproteins of other cytoplasmic and vacuolar membranes (Millet, 2010, Millet et al. 2013). These fluorophores also enter membrane-bound neutral lipid droplets and partition into their contents (Fig. 4f). Tetramethyl-rhodamine ethyl (or methyl) esters are more specific for hydrogenosomal uptake (Williams et al., 2013a). An alternative is the tetrazolium salt CTC (5-cyano-2, 3-di-(*p*-tolyl) tetrazolium Cl) with permeant properties (Sockert et al., 2018), and with a redox potential appropriate for reduction to a red fluorescent formazan product by flavin-mediated electron transport.

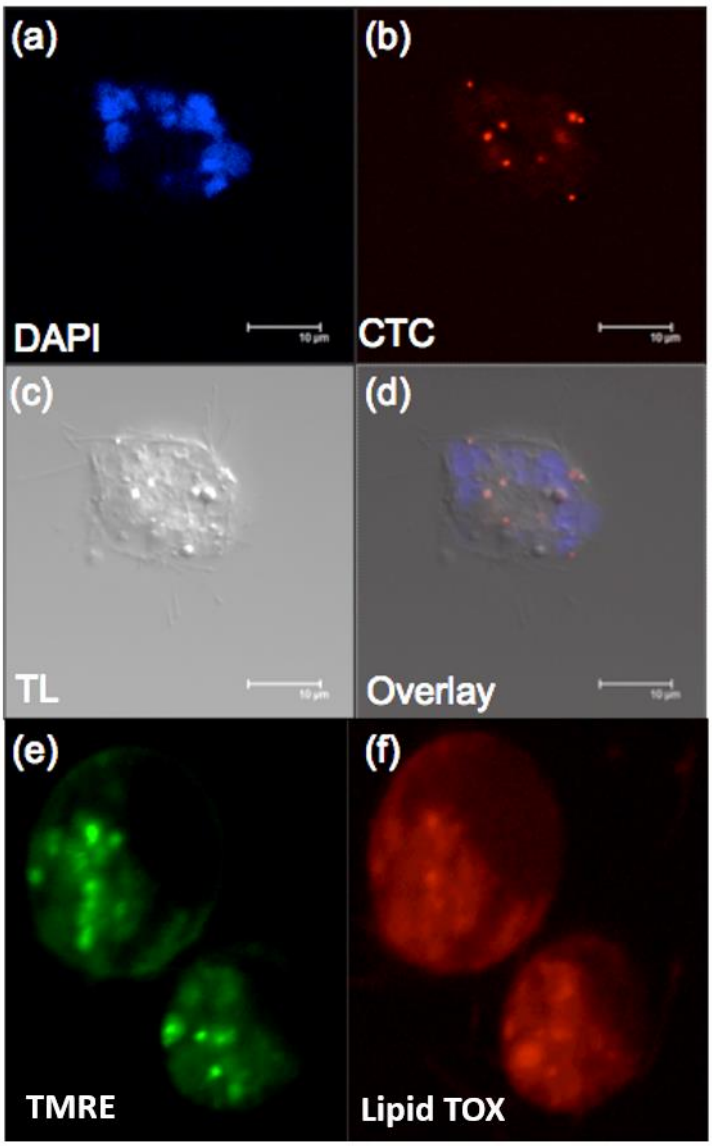

Fig. 4. Live cell fluorescence imaging of *S. vortens* using 2% (w/v) chloral hydrate solution to restrict motility and intracellular motion, and a reactive oxygen species scavenger (DABCO) to minimize photobleaching. (a) DAPI (DNA, RNA, in paired nuclei); (b) CTC: tetrazolium reduction product in hydrogenosomes (a fluorescent formazan); (c) Nomarski phase contrast transmission image; (d) overlay of a, b and c; (e) TMRE: tetramethyl rhodamine ethyl ester for $\Delta\varphi$, hydrogenosomal transmembrane electrochemical potential. (f). Lipid TOX™

3.4 Some newly designed and applied luminophores

Fluorescent propargyl-functionalised 1,8-naphthalimide conjugates used as cellular imaging agents indicate that the uptake and intracellular localization of these probes both in human osteoarthritic cells and in *S. vortens* is dictated by the specific nature of the naphthalimide structure (Langdon-Jones et al., 2014). Gold(I) coordinated complexes of these systems retained the visible fluorescence, via intramolecular charge-transfer, of the 1,8-naphthilamide ligand and their potential for labeling HEK (human embryonic kidney) cells and *S. vortens* using confocal microscopy was demonstrated (Fig. 5). Favourably low toxicities, emission maxima ca. 540nm, lifetimes up to ca.10ns, and with quantum yields >50% further indicate their usefulness in this context (Langdon-Jones et al., 2015).

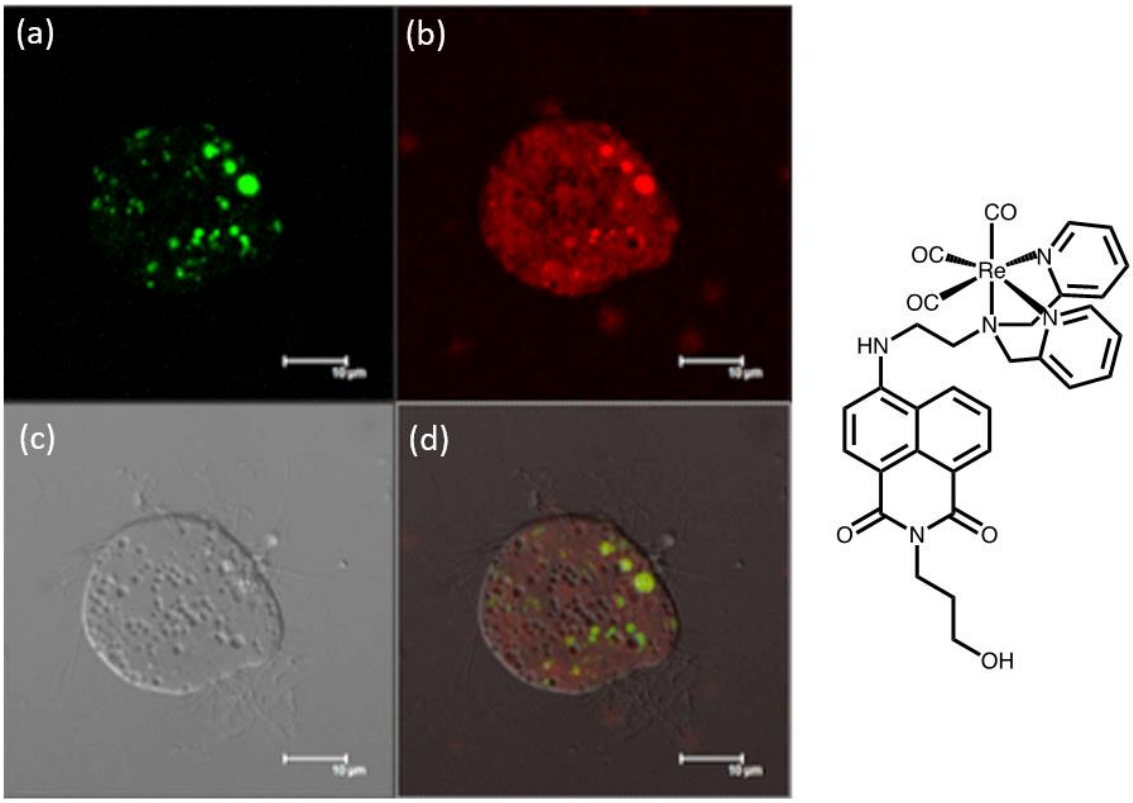

Fig. 5. Images of large form of *S. vortens* incubated with Re-L^2 and TMRE showing (clockwise from top left): green fluorescence from Re-L^2 (λ_{ex} = 488nm; λ_{em}
= 515nm); red fluorescence from TMRE (λ_{ex} = 543nm; λ_{em}

= 600nm); overlaid images showing co-localisation; Nomarski phase transmission image. (Langdon-Jones et al., 2014)

A series of related picolyl-functionalised fluorescent 1,8-naphthalimide ligands (L) can be coordinated to Re(I) to give fluorescent cationic complexes, with the 4-amino derivatives again exhibiting intramolecular charge-transfer in the visible spectrum. Both the entry into and intracellular localization in fission yeast of selected complexes were dependent upon the specifics of the ligand structure (Langdon-Jones et al., 2017b).
The synthesis and luminescent properties of a series of related cationic dihydroimidazolinium functionalised 1,8-naphthalimides have also been investigated. These fluorophores can be deprotonated to act as N-heterocyclic carbene donors for coordination to Au(I). Both the cationic pro-ligands and the charge neutral Au(I) complexes prove to be useful imaging agents (Fig. 6., Groves et al., 2019). These species can also be applied to FLIM studies as their lifetimes are modified by the presence of coordinated Au(I) thereby validating the integrity of the metal-ligand complex when present in the cell. In Fig.7. (Groves et al., 2019), the predominant fitted lifetime of 11 ns determined intracellularly is much longer than that obtained spectroscopically (1.1ns), suggesting that the Au(I) complex may dissociate under the ambient conditions within the carcinoma cell.

In further developments, highly conjugated azonafide inspired anthracene-1,9-dicarboximide fluorophores have also been developed (Langdon-Jones et al., 2017a). In a similar fashion, these fluorophores were functionalised with a dipicolylamine chelate, providing a coordination site for a metal ion (in this case Re(I)) and imparting a cationic charge upon the probe. These compounds show anticancer properties against a variety of cell lines (LOVO, A549, PC3, MCF7), but are not as potent agents for chemotherapy as that of azonafide, the lead compound of the series. Critically, the study demonstrated the viability of the anthracene-1,9-dicarboximide fluorophore in a cell imaging context with MCF7 and fission yeast.

These species fluoresce at ca. 500 nm with lifetimes up to 16 ns, as well as showing concentration dependent emission behaviour likely driven by aggregation.

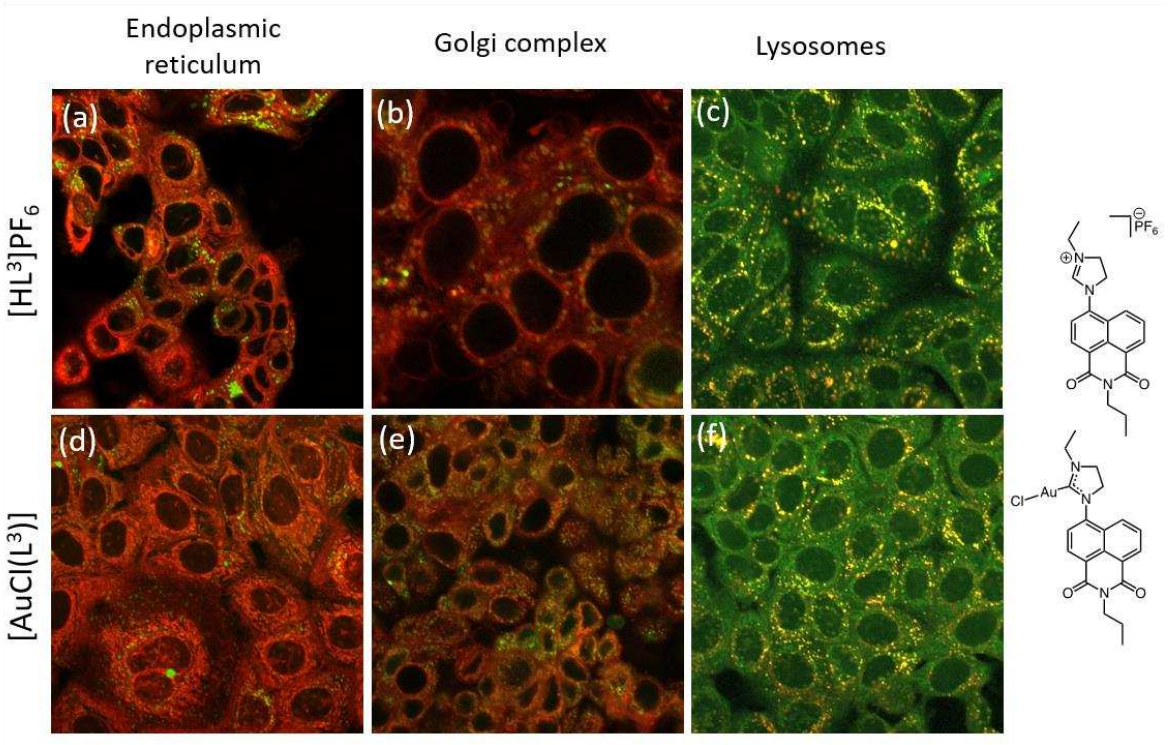

Fig.6. Cultured Human MCF-7 cells (breast adenocarcinoma) incubated with $[HL^3]PF_6$(top) and $[AuCl(L^3)]$ (bottom). Representative superimposed images where yellow-orange signifies co-localisation (from left to right) with endoplasmic reticulum, Golgi and lysosomal specific fluorophores respectively. Note strong lysosomal co-localisation (Groves et al., 2019).

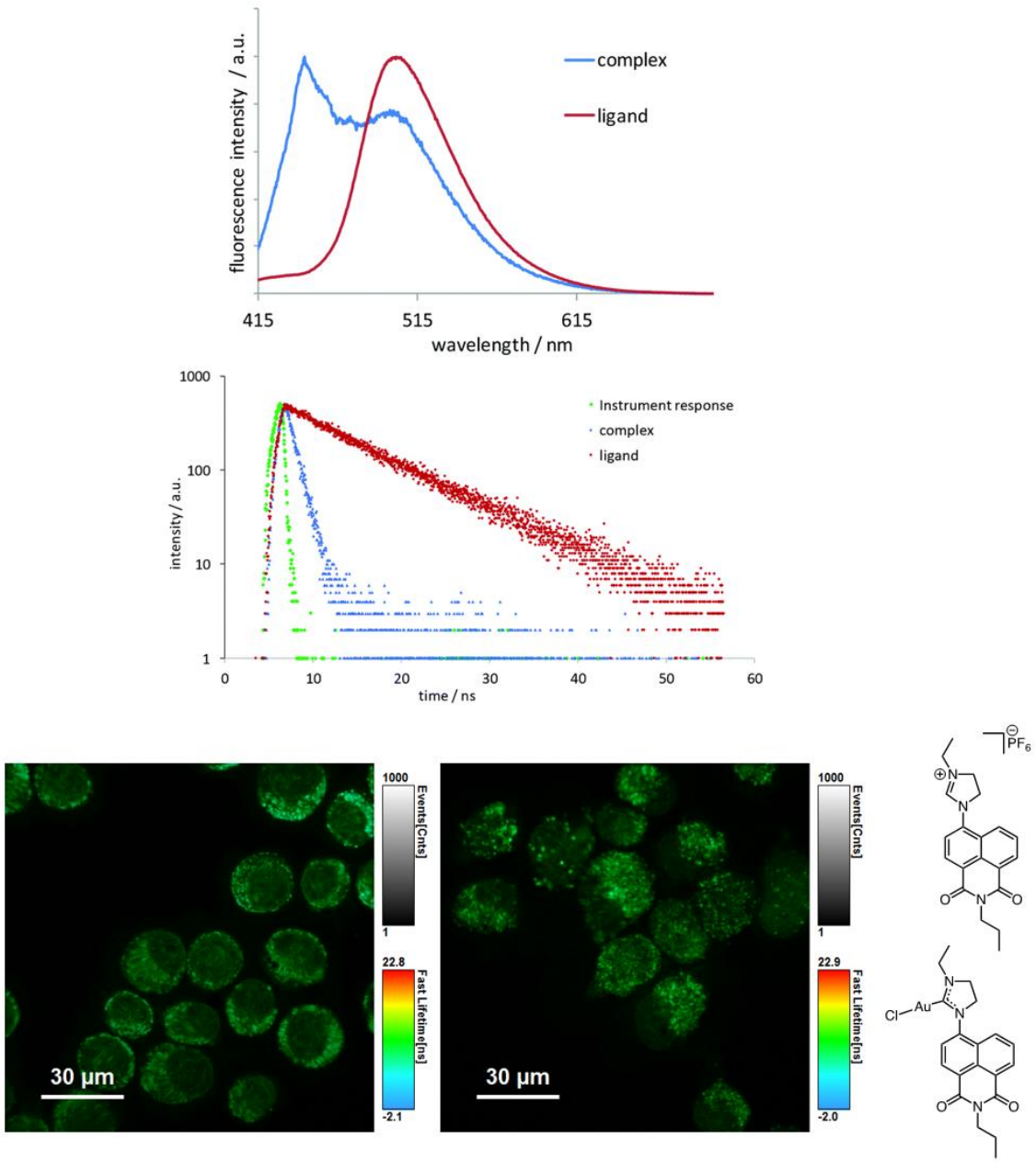

Fig. 7a. Top: Normalised emission spectra of selected complexes excited at 405 nm (recorded in aerated acetone). Bottom: Time resolved measurements showing the comparative decay profiles for ligand $[HL^3]PF_6$ (red) and complex $[AuCl(L^3)]$ (blue) against the instrument response (green).

b. FLIM images of MCF-7 cells incubated with $[HL^3]PF_6$ (left), and $[AuCl(L^3)]$ (right) using pulsed excitation at 440nm.

Fitted parameters (left): $\tau_1 = 9.2$ ns (77%), $\tau_2 = 3.4$ ns (20%), $\tau_3 = 0.4$ns (3%); (right): $\tau_1 = 11.0$ns (68%). $\tau_2 = 3.9$ ns (25%), $\tau_3 = 0.5$ns (7%) (Groves et al., 2019).

3.5 Phosphorescent probes

There is special importance and interest in low-energy emission IR probes as the depth of penetration into cells and tissues is increased and photochemical damage diminished over that of shorter wavelengths (Lloyd et al., 2012).

Late transition (often d^6)-metal complexes, especially as their polypyridyl complexes, have been extensively employed in biological imaging: rhenium(I) (Amoroso et al., 2007, 2008a, Lo et al, 2008a), ruthenium(II) (Lo et al., 2008b), and iridium(III) (Yu et al., 2008) have been prominent in many applications.

A series of rhenium *fac*-tricarbonylbisimine complexes of varying charges and lipophilicities were tested as suitable for use as luminophores in yeasts and mammalian cells. Uptake and photochemical stability were in general good, and short-term toxicity was negligible so that ground-rules for acceptability as useful phosphors were established.

Luminescent, water soluble gold nanoparticles functionalized with ^{3}MLCT emitting rhenium complexes, retain emission to a greater extent than many other preparations employing organic tethers, and thereby showing promise for uses in bioimaging applications (Hallett et al., 2009).

An exceptionally interesting development (Coogan et al., 2009) related to this work resulted in the formation of a molecular cationic 'vessel', impermeant to the cytoplasmic membrane when empty, but enabled to carry metal ions through the limiting cytoplasmic membranes of MCF cells (Thorp-Greenwood et al., 2011). Co-localisation with SYTO®RNASelect, a fluorescent marker for nucleoli, demonstrated the transport of the complex with silver ions within the 'Sleeping Trojan Horse' into this specific compartment of the nuclei. Potential for bimodal luminescence/radioimaging is indicated.

Photoemissive lanthanide ions (e.g., complexes of europium(III), terbium(III) and samarium (III) are visibly luminescent (Eliseeva and Bunzli, 2010), whilst neodymium(III), whilst erbium(III), and ytterbium(III) show near-IR phosphorescence (Faulkner et al., 2005). One tuneable example of a red-to-near IR emitting luminophore is a platinum trimethyl

bipyridyl thiolate (Steel et al., 2015), exhibiting an unusual inter-ligand charge Transfer (ILCT) transition.

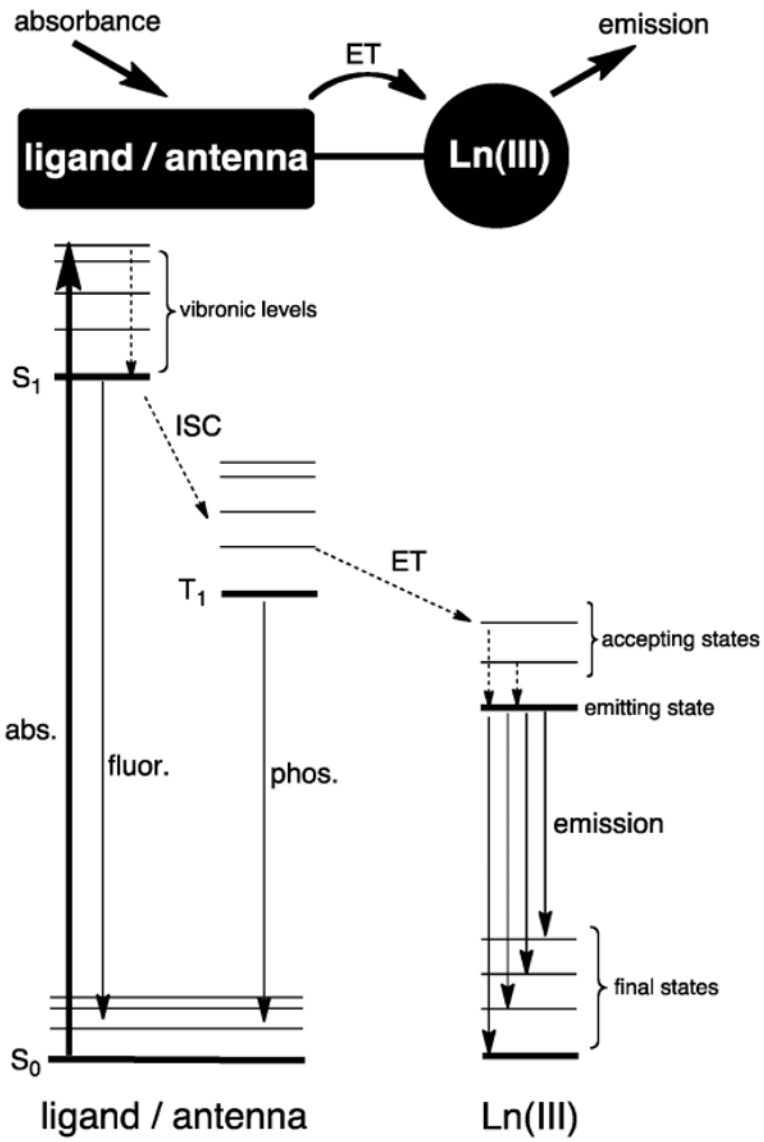

Fig. 8. A simplified model for sensitized lanthanide luminescence, and energy-level diagram for an emissive chromophore-appended lanthanide complex sensitized via a ligand-centred triplet excited state (abs = absorbance, fluor = fluorescence, phos = phosphorescence, ISC=intersystem crossing , ET= energy transfer (Amoroso & Pope, 2015).

Transition metal luminophores, with well established favourable physical properties and chemical stability currently abound, but as indicated (above), for practical uses as cellular imaging reagents, must also be taken up into cells, show defined intracellular

localizations, be minimally perturbing to metabolism, and to long term cell viability. Imaging agents based on the *fac*-{$Re(CO)_3$}bipyridine core have proven highly amenable to controlled manipulation (Balasingham et al., 2011) especially when linked through functionalized alkyl chains (Balasingham et al., 2012).

Near-IR emitting lanthanide complexes serve as both water-soluble metal-ion modulated luminescent probes and magnetic resonance contrast agents (Fig.9; Andrews et al., 2011), and thus promise useful as bi-modal applications in biology.

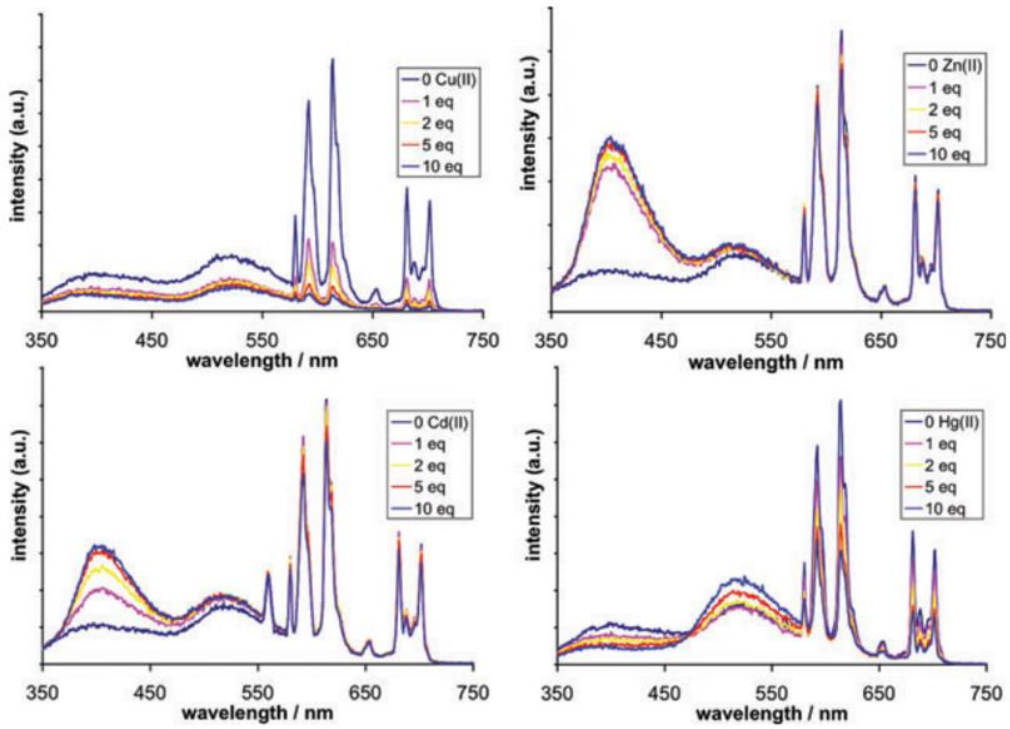

Fig. 9. Steady state emission spectra for Eu-L^b (10^{-5} M) in the presence of (clockwise from top left) of Cu^{II}, Zn^{II}, Hg^{II}, and Cd^{II}. Recorded in buffered water, pH7.4 (Andrews et al., 2011).

DNA- rhenium dppz binding complexes can be appended through the axial pyridine by a range of substituted pyridines. These complexes can gain organelle specific localization (i.e., in mitochondria or in nuclei) while retaining their intense phosphorescence (Fernández-Moreira et al., 2010a,b), e.g., in HeLa cells (Thorp-Greenwood et al., 2012, Coogan & Fernández-Moreira,

2014. Nucleoli can be similarly targeted (Thorp-Greenwood et al., 2011).

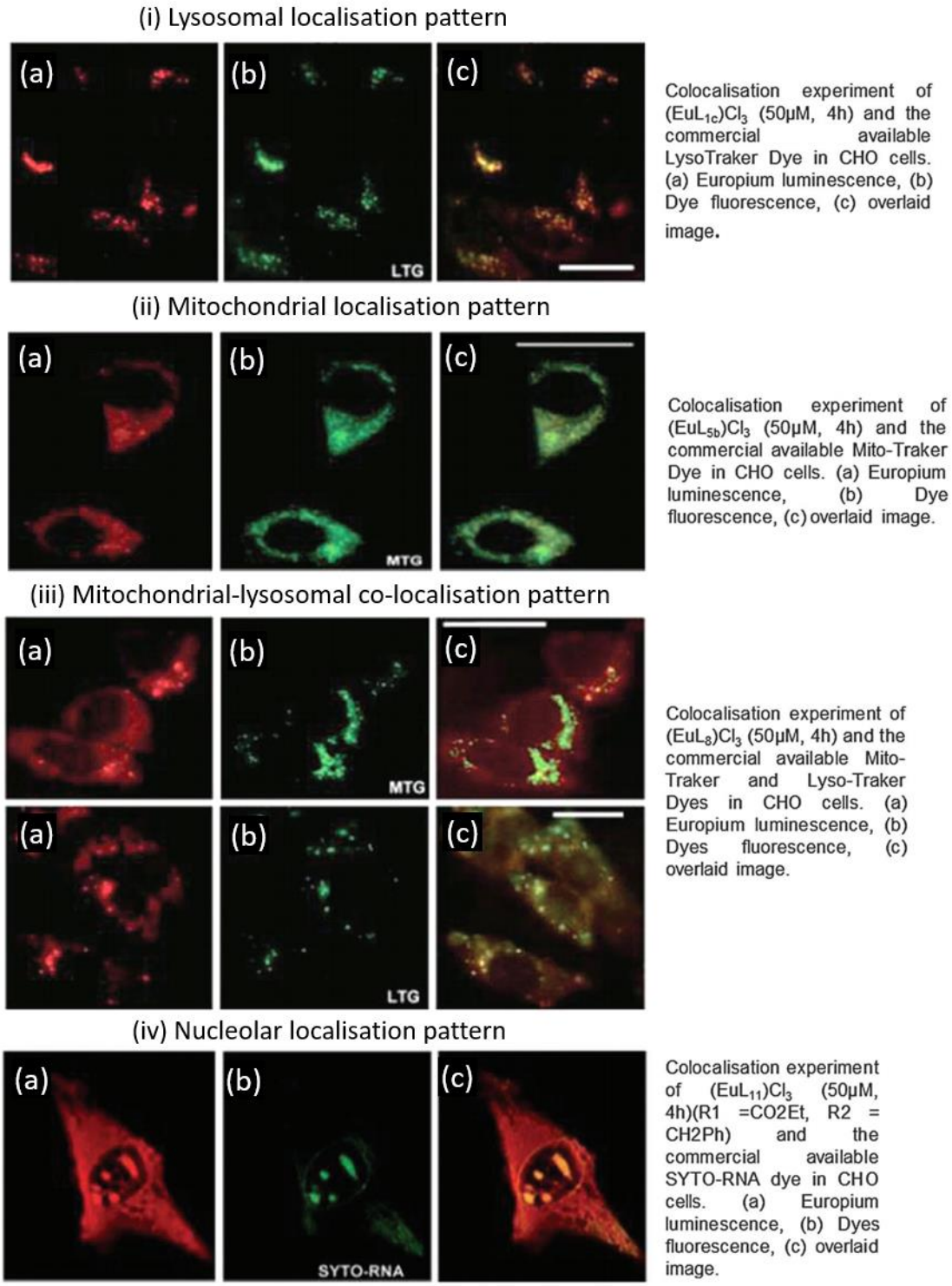

Fig. 10. Fluorescence microscopy of several lanthanide probes colocalised with corresponding commercially available probes to visualize specific sub-cellular localisations, New & Parker, 2009; Coogan & Fernández-Moreira, 2014.

A systematic study was carried out on the role of hydrophobicity of amphiphilic rhenium bipyridyl complexes bearing axial substituted imidazole or thiazole ligands on their cellular uptake and the subsequent viability of organisms. The fission yeast, *Schizosaccharomyces pombe,* and *S. vortens* acted as model organisms (Hallett et al., 2018). In both cell types access to the nuclear compartments was promoted with increasing lipophilicity, whereas increased chain lengths gave greater toxicities. Complexes of the most lipophilic ligands could potentially be adapted for use as radio-imaging agents(e.g., as ^{99m}Tc(I) analogues while still being useful using confocal microscopy in cellular imaging studies.
Zirconium and hafnium metallocene dihalides based on simple polyphenyl cyclopentadienes with a large Stokes shifts and good room temperature stability with emission from triplet states are also promising cell imaging compounds (Pritchard et al., 2013). Incubation with MCF-7 human adenocarcinoma gave images showing incorporation into peripheral extra-nuclear organelles and satisfactory maintenance of cellular integrity indicated low toxicity Application of phosphorescence imaging to *S. vortens* has proved useful in the selection of complexes of freely permeable derivatives with toxicity characteristics with emission well separated from routinely employed fluorescent probes, thereby enabling co-localisation studies. The extended phosphorescent lifetimes (i.e., μs rather than ns for fluorescence) also provides for further discrimination from or identity with intracellular localization of fluorescent probes employed as established markers for known organelles. An example of a luminescent Pt-Yb water soluble cyclometalated conjugate when excited at 355nm shows maximal emission at 997nm with a lifetime of 902ns, that was attributed to the Yb(III) ion. The Pt(II) complex part of the molecule showed a corresponding lifetime of 50ns at 619nm (Stacey et al., 2015). This Pt-Yb dimetallic species was successfully applied to cell imaging using fission yeast.

The highly sensitive quenching of phosphorescence by di-oxygen has been extensively exploited as a method for measurement of O_2 concentrations within tissues, body fluids and cells, but this approach is hampered by sensitivity of emission to ambient

conditions of pH, ionic composition and local hydrophobicity. To minimize these perturbing effects, nanoparticles of diameter 45nm, containing polyacrylamide-embedded $[Ru(dpp(SO_3Na_2)_3)]Cl_2$, were electroporated into model yeasts, or into cultured mammalian cells (Coogan et al., 2010). Reversible quenching of ^{3}MLCT phosphorescence as measured at 650nm was observed during anaerobic-aerobic transitions.

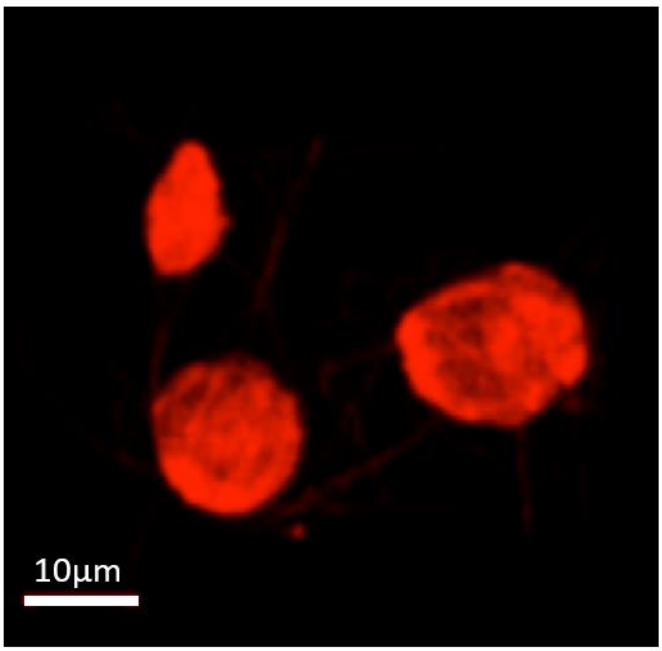

Fig. 11. Two-photon excited laser scanning microscope images of nanoparticle encapsulated Ru-coordinate complex electroporated into *Spironucleus vortens*. The scale bar = 10µm (Lloyd et al., 2014).

Controlled conditions of electroporation of nanoparticles (340 V, 900 µF, 200 ohms in a 2mm path length) into cells gives reasonable preservation of ultrastructure and function, thus the motility of *S.vortens,* and also the NAD(P)H content of both yeast and cardiomyocytes, all survive the procedures of the technique (Williams et al., 2012b, Lloyd et al., 2014). Two-photon excitation at 900nm was used to image organisms and cells in this study

whereby phosphorescence lifetimes were correlated with intracellular O_2 concentrations.

Further examples of novel luminophores are provided below in Figs. 12-14): Jones and Pope (2009; Jones et al., 2011, 2012); Felton et al., 2008.

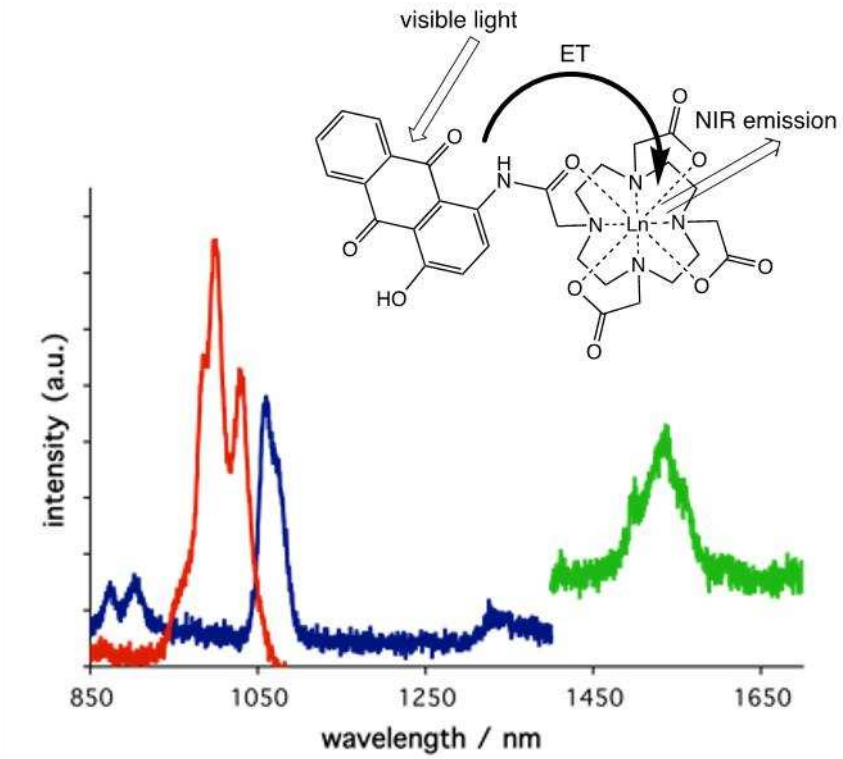

Fig. 12. Steady state emission spectra for **Ln-L2** (red, Yb; blue, Nd; light green, Er) measured in D_2O using λ_{ex} = 450nm. Spectra offset for clarity, Jones and Pope (2009).

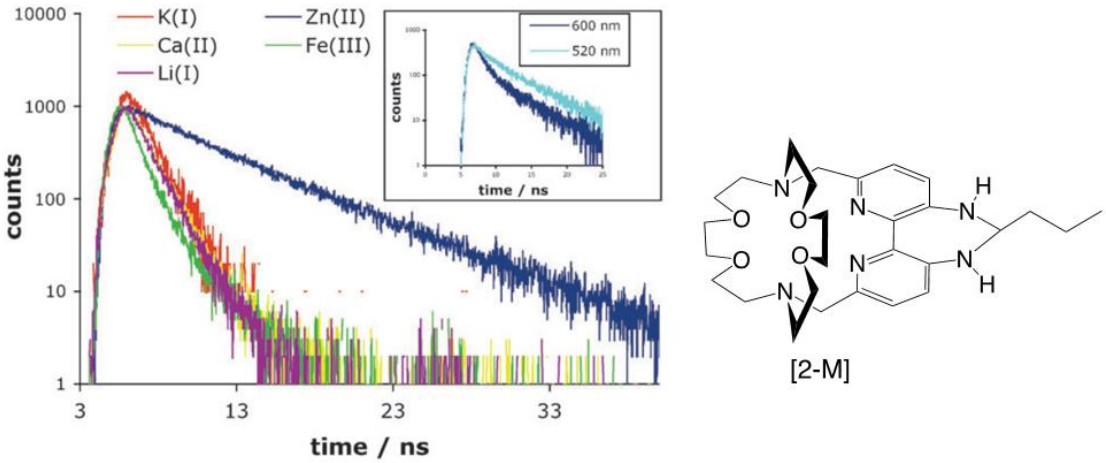

Fig. 13. Comparative luminescence decay profiles of [2-M] $^{n+}$ where M = K^{+}, Zn^{2+}, Fe^{3+}, Ca^{2+}, Li^{+}. Inset: wavelength dependent lifetime decays of [2M] $^{n+}$ in an ionic mixture. Data fits and residuals are omitted for clarity. Felton et al., (2008).

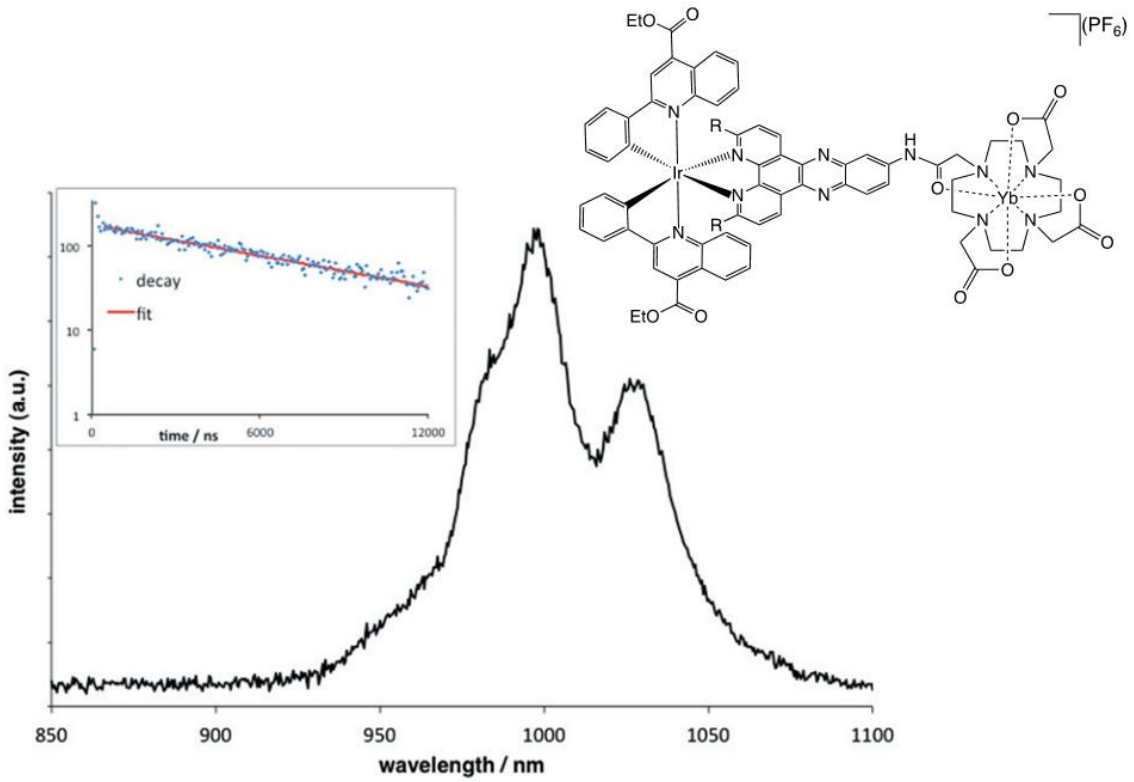

Fig. 14. Near-IR emission spectrum of [Ir-L^{8}-Yb](PF6) recorded in D_2O (λ_{ex} = 410nm). Inset corresponding lifetime decay at 980nm in D_2O (Jones et al., 2012).

4. Imaging of fixed organisms

4.1 Ca^{2+} binding sites

Major roles for calcium in cellular structural integrity as well as in metabolic and signaling functions make bound Ca^{2+} ions useful markers for optical microscopical investigations (Gerencśer & Adam-Visi, 2001, Gerencśer et al., 2005, 2012, 2017).
Calcium ions and channels are necessary for a wide variety of basic transport functions associated with intracellular and extracellular compartmentation (Evans, 2006, Campbell, 2017). Thus, as well as their vital roles in mitochondrial, endoplasmic reticulum, endosomal, Golgi and ectosomal functions, they also participate in the control cell division cycle progression cytokinesis, and differentiation (Senatore et al., 2016) as well as motility (Doerner et al., 2015). They also act within mitochondria (Carafoli & Krebs, 2016), and hydrogenosomes, (Humphreys et al., 1994, 1998), and a plethora of specialized organelles for life in highly specialized, variable, and sometimes stressful environments. Examples of the latter are manifest in gravitaxis (Häder & Hemmersbach, 2017), mineral nucleation (Omelon et al., 2013, Liu et al. 2018) and acidocalcisomes (Docampo et al., 2013). The ubiquity of bound calcium in *S. vortens* and its persistence after formalin or ethanol fixation in cellular structures have prompted our extensive use of X-Rhod, 5F, AM, a fluorogen first employed by Gerencśer & Adam-Visi (2001) as an outstandingly revealing agent of the morphology of this protist.

4.1.1 Fluorescence measurements of *S. vortens* suspensions after preincubation with X-Rhod, 5F, AM

In Figure15 (A) Fluorescence emission spectrum typical of *S. vortens* pre-incubated with 5 μM X-Rhod, 5F, AM for 1 h at 30°C. (B) Additions of 1 mM EDTA, K_d (Ca^{2+}) = 0.4nM gave typical intensity decreases that accompany fluorescence emission transients

in these suspensions. Three successive additions of 74 µM Adalat (Bayer, BAY a1040, Nifedipine), a dihydropyridine L-type calcium channel (also a non-specific voltage-gated-dependent calcium channel inhibitor, McDonald et al., 1994) gave further decreases in fluorescence. Restoration of emission occurred on addition of 2 successive additions of 1 mM $CaCl_2$ followed by a gradual increase, indicating that incomplete intracellular hydrolysis of the acetyl methoxy-fluorophore derivative during pre-incubation. The organisms were still fully motile at the end of this experiment and 1 day later.

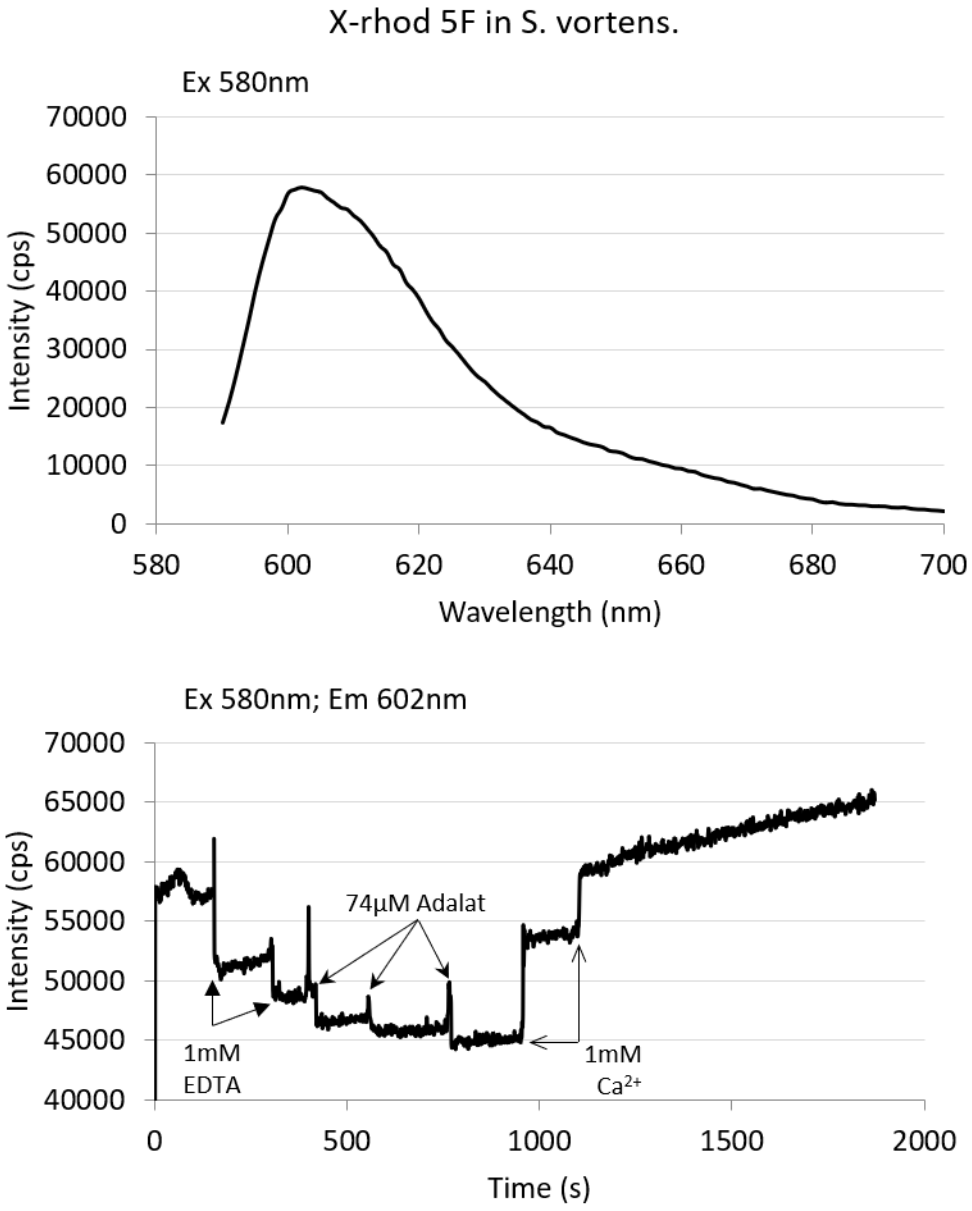

Fig. 15. (A)The fluorescence emission spectrum of *S. vortens* suspensions after preincubation with X-Rhod, 5F, AM are shown. (B) Effects of EDTA, Ca^{2+} channel inhibitor, and Ca^{2+} additions.

4.1.2 Confocal microscopy of Ca^{2+} binding sites in *S. vortens*

The presence of hydroxyl-apatite (calcium hydroxy phosphate) granules in mitochondria has been noted for more than 60 years, and two classes of mitochondria identified in a wide variety of organisms characterized by their different calcium-binding properties (Carafoli & Lehninger, 1971) The first group includes those from many vertebrate tissues, with a specific extremely high-affinity carrier for, and a rapid respiratory response to Ca^{2+} and accompanying rapid cation uptake and proton ejection, whereas the second group exhibit low affinity for Ca^{2+}, and respiratory responses and ion transport are slow or effectively absent. Mitochondria from yeast most resemble the second category (Carafoli et al., 1970). These and subsequent investigations also concluded that yeast mitochondria lack a specific Ca^{2+} carrier and that the physiological significance of transport at high (1-10 μM) concentrations is uncertain (Lloyd, 1974).
In trichomonads, the hydrogenosomes (Chapman et al., 1986a; Humphreys et al., 1994, 1998) as in those in *Neocalimastix frontalis*, a rumen fungus (Biagini et al., 1997c) and *Metopus contortus*, a sediment dwelling freshwater ciliate (Biagini et al., 1997d) have accumulated stored Ca^{2+} as distinct granules.
Calcium specific antibody-binding has indicated that annexins of *S. salmonicida* are related to alpha-giardins (Weiland et al., 2005, Wenman et al., 1993) but evolved with better-preserved type II calcium coordination sites (Einarrson et al., 2016). Two annexins bind to phospholipids in a calcium-dependent fashion but with individual specificities. Super-resolution and confocal microscopy

of epitope-tagged *S. salmonicida* annexins revealed localization to distinct parts of the cytoskeleton and cell membrane. The ultrastructural details of the localization of several annexins were determined by proximity labeling and transmission electron microscopy. Two annexins localized to a novel cytoskeletal structure in the anterior of the cell. These results also showed that the annexin gene family is expanded in diplomonads, and that these group E annexins are associated mostly with cytoskeletal and membrane structures in *S. salmonis.*

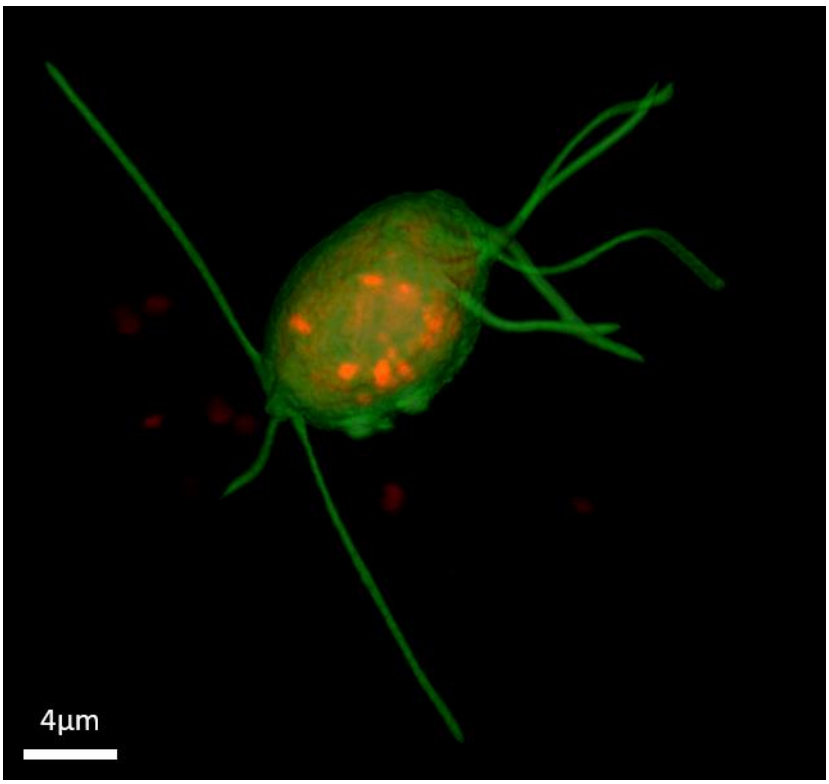

Fig. 16. Anaesthetised *S. vortens* after incubation in growth medium, after 1.5h preincubation with X-Rhod, 5F, AM, and still showing slight flagellar movements. Calcium binding sites in numerous organelles and widely distributed very small vacuoles.

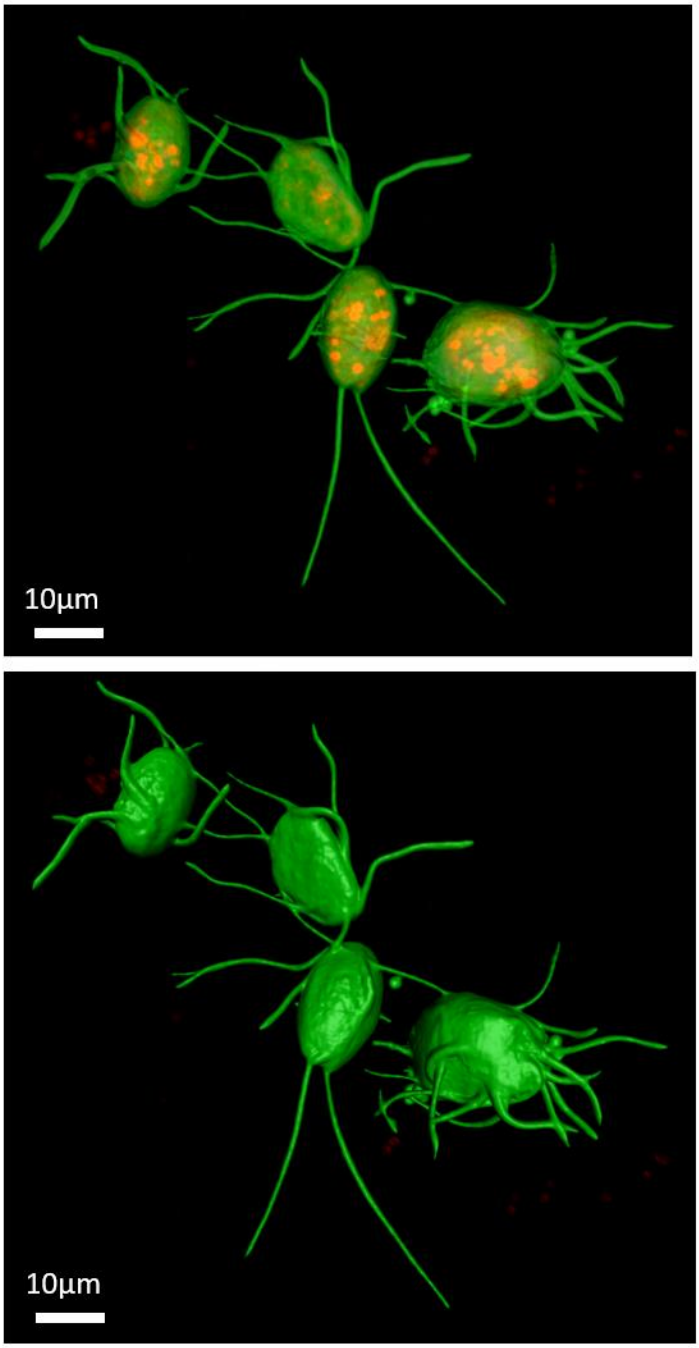

Fig. 17. Surface-rendered 3D optical images of fixed and washed *Spironucleus vortens* generated from a z-plane section stack (mean section thickness 0.4µm), after uptake and de-esterification of X-Rhod 5F, AM for 1.5 h; then plus 1mM $CaCl_2$, followed by 1.0mM EDTA and fixation in 3% formaldehyde in PBS. This shows a group of organisms each with 6 lateral and 2 posterior flagella and the arrangement of the 16 flagella in a single organism about to divide, the latter organism was used to generate the data seen in Figure. 18. Colour-coding (green) reveals the surface structure, and organelles (red) having the highest internal residual Ca^{2+} concentrations i.e., the smaller hydrogenosomes, and larger lipid droplets and more diffuse nuclear phospholipid-rich membranes.

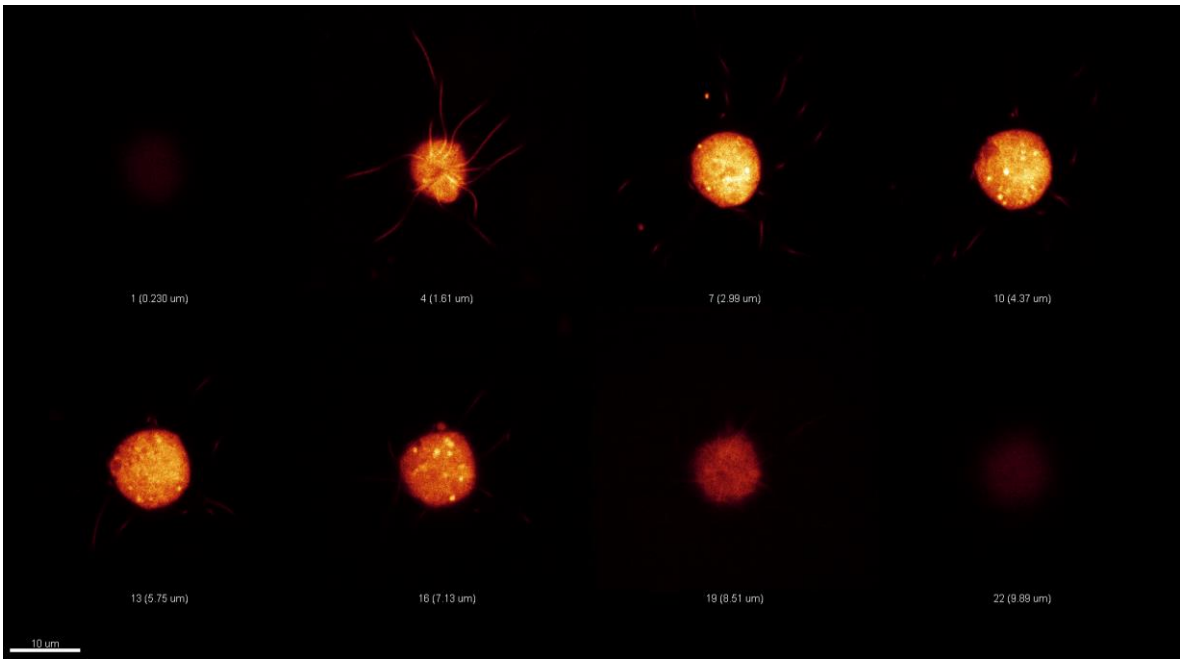

Fig. 18. Surface characteristics of the same group of organisms fixed and fluorophore treated exactly as in Fig.17, but only coded for surface features.

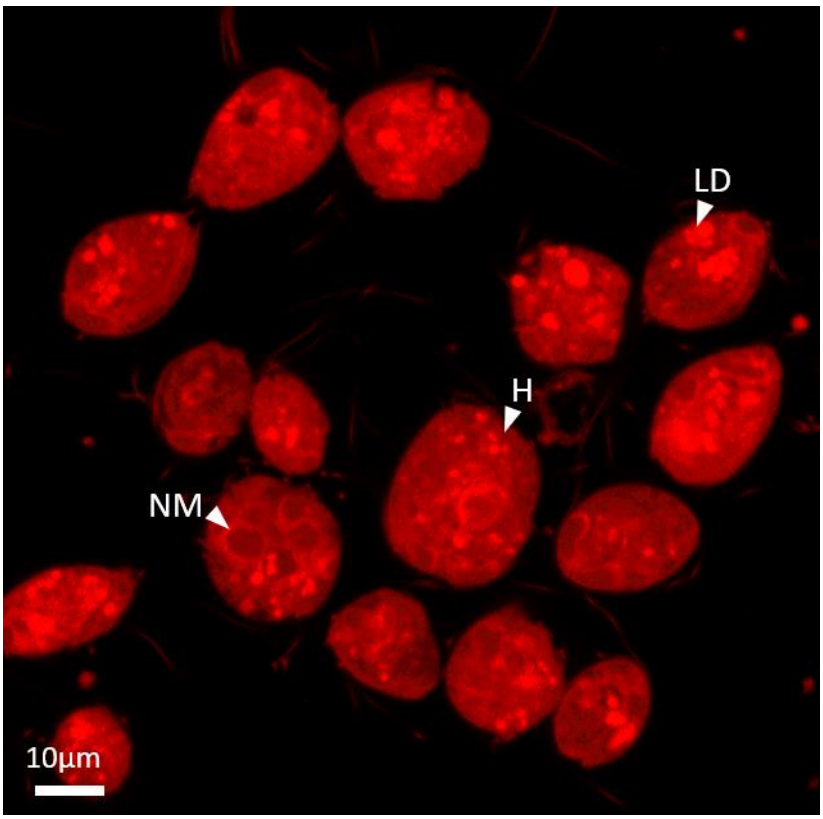

Fig. 19. Treatments as in Fig. 17. A single section through a group of organisms selected to show organisation of internal membranes and organelles , hydrogenosomes, (H) lipid droplets (LD), nuclear membranes (NM), and closely packed small vacuoles and diffuse cytoplasmic labeling . Some released hydrogenosomes from damaged organisms are also present. Scale bar = 10µm.

4.2 Simultaneous CARS/SHG imaging

A single 5fs Ti sapphire broadband (660-970 nm) laser enables the simultaneous acquisitions of Coherent Anti-Stokes Raman Scattering (CARS), 2-photon fluorescence and second harmonic generation (SHG) imaging, providing a novel and useful instrument for combined studies of cellular ultrastructure and function (Fig.17, Pope et al., 2013). The in-house house developed system is based around a commercial Nikon Ti-U inverted microscope, also enabling conventional brightfield, differential interference contrast (DIC) and epifluorescence imaging of biological material. For an explanation of the principles behind CARS and the different experimental techniques see for example Pope et al., 2012.

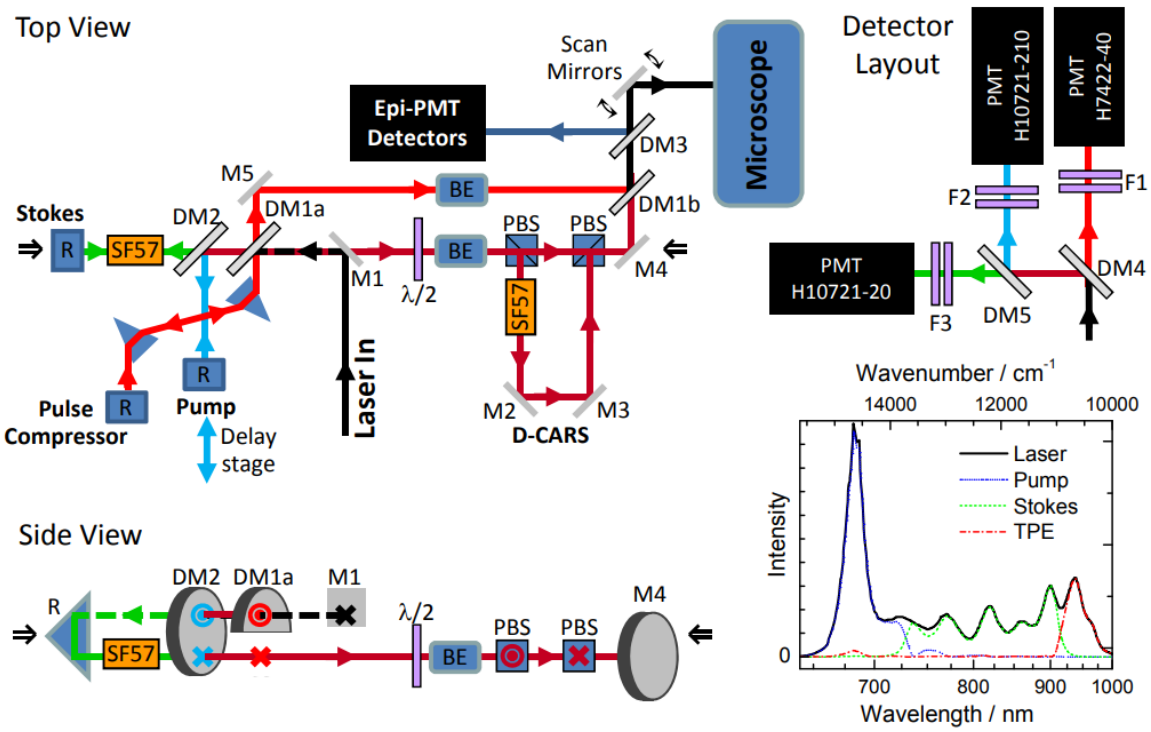

Fig.20. CARS and SHG images were acquired using the experimental setup shown above: M, mirror; DM dichroic mirror; SP57 glass block; R reflecting prism; λ/2 half-wave plate; BE beam expander; PBS polarizing beam splitter; F filter; The side-view of the optics between the two indicated arrows show the beam height difference. Graph: typical spectra of the laser and splitting into the pump, Stokes and TPE beams. (Pope, I. et al., (2013)

Saturated and unsaturated fatty droplets can be imaged and distinguished using this technique via spectral analyses of hyperspectral image stacks (DiNapoli et al., 2014a). This technology has thus been extensively employed to study human adipose-derived stem cells (DiNapoli et al., 2014b), especially the participation of lipid droplets in adipogenesis (DiNapoli et al., 2016). The roles of fatty acid and pyruvate at different stages in lipid storage and utilization in mouse eggs have also been elucidated (Bradley et al., 2016, 2019).

To investigate the chemical content of the *S. vortens* simultaneous CARS and SHG imaging was undertake on formaldehyde fixed *S. vortens*, mounted in water between a cover slip and glass slide using a 120 micron thick image spacer (Grace Biolabs). A single frequency (2830 cm^{-1}) CARS image of two *S. vortens* is shown in Fig. 21(a). The dashed yellow line indicates the point where a CARS line scan (over the spectral range 2100 cm^{-1} to 4000 cm^{-1}) was taken, cutting through a prominent droplet in the upper most *S. vorten* as well as cytosolic regions. The line scan information is displayed in Fig. 21(b) as a 2D image with increasing wavenumber from left to right of the image and spatial information contained in the vertical direction. For reference, three regions of interest are identified by coloured stars in the single frequency CARS image (Fig. 21(a)) and the corresponding parts of the line scan image (Fig.21 (b)). The boxes indicated on the line scan image show the regions over which the data were averaged to generate the spectra displayed in Fig. 21(c). Looking at Fig.21(c) left, we see that the spectrum L1 (black) associated with the prominent droplet is dominated by a strong lipid component whereas, spectrum L2 (red) has a distinctly different shape associated with the cytosolic region (cytosolic proteins). Spectrum W, corresponding to the region in

between the two *S. vortens* and shows the typical water spectrum, as expected. The influence of the water spectrum can also be seen in both spectra L1 and L2, this is due to the addition of water within the focal volume of the objective. Fig.21(c) right, shows spectra L1 and L2 with the water component subtracted.

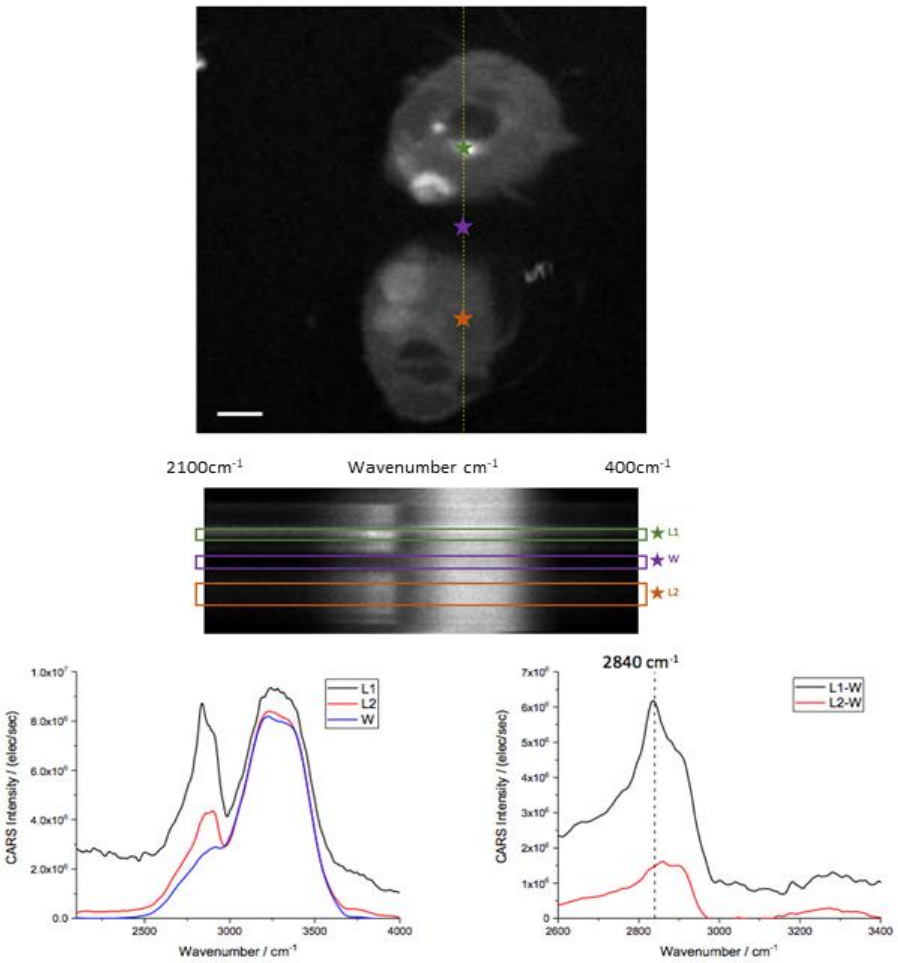

.

Fig. 21. (a). *S. vortens*: a CARS image (20 x 20 µm) taken at a vibrational resonance = 2830 cm^{-1} (scale bar =2µm): the yellow dashed line indicates the region where a hyperspectral line cut was taken. Stars indicate points from where spectra were taken. (b). The CARS line scan taken across the region of the yellow dashed line, in (a). The line covers the vibrational range from 2100 cm^{-1} to 4000 cm^{-1}, thereby extending beyond the filter range (2500 cm^{-1} to 3800 cm^{-1}), so that background levels can be determined. (c). The graph (left) shows the spectra averaged over the regions identified by the boxes in (b); The graph (right) shows the same data as in the graph to the to the left with the water spectrum (W, with a peak centered around 3270 cm-1) subtracted. The spectrum L1 has a familiar lipid profile with a maximum at around 2840cm^{-1}.

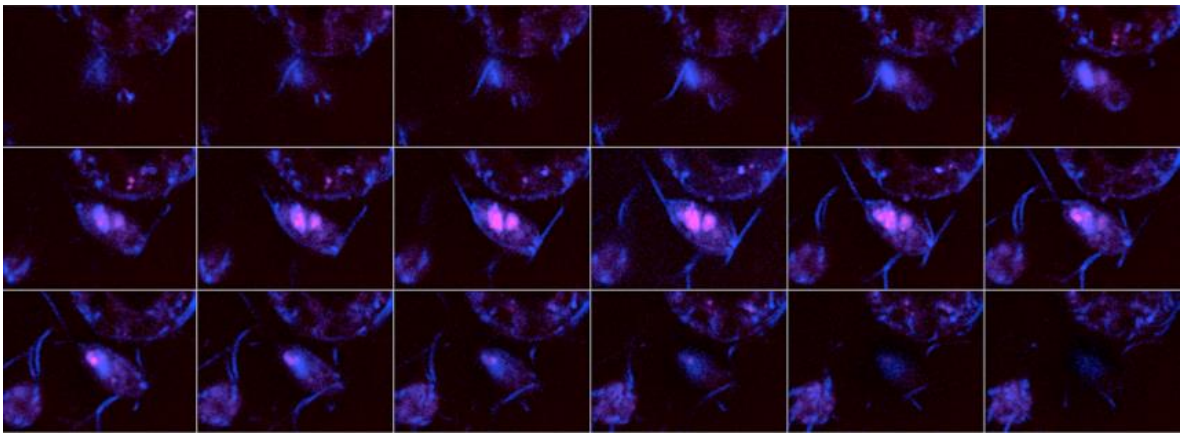

Fig.22. The montage above shows a series of z-slices (0.5 µm apart) through the *S. vortens* centred in the image. Each individual image is 29 x 21 µm (289 x 210 pixels) and shows simultaneously acquired CARS at 2850 cm^{-1} (red) and SHG (blue). See Supplementary 4 for movies of the z-stack and 3D reconstruction.

5. Discussion

The rapid motility of *Spironucleus vortens* is characteristic in the identification of this organism (Williams et al., 2013b, Lloyd et al, 2015). The trophozoite reaches velocities of 161µm/s or 13.3 body lengths/s (mean of 16 measurements, data not shown). Both this

rapid motility (Supplementary 1) and the dynamic state of the intracellular contents (Supplementary 2), makes live cell imaging involving this organism challenging.

Lipid droplets although ubiquitously recognized in the cells of eukaryotic organisms, are only relatively recently studied intensively e.g., in yeast (Wolinski et al., 2009, 2011). CARS and SHG imaging is providing new insights into the formation and utilization of their contents as dynamic sources of energy for cellular growth and development (Di Napoli et al., 2014a, b, c, Bradley et al., 2016, 2019).

For future studies the smaller vacuolar structures and their contents, endosomes, Golgi membranes, endoplasmic reticulum, lysosomes ('acidic calcium stores') and exosomes fluorescing with the calcium binding indicator observed here and also evident in electron micrographs of *S. vortens*, (Poynton & Sterud, 2002, Poynton et al. 2005, Millet et al., 2011, Williams et al., 2013a) require further work.

In this respect use of newly developing fluors and phosphors as well as immunological detection (e.g., by the use of annexin specific antibodies) are likely to be very informative. Supplementary and more definitive resolution of organelle and membrane structure and functions will require disruption, subcellular fractionation and biochemical studies. Fluorescence imaging using the methods previously shown to specifically reveal, identify and characterise regions of elevated Ca^{2+} in intracellular compartments (Gerasimenko et al., 1998), and membranes in cultured mammalian cells (Gerencser et al.,2012, 2017, Lloyd-Evans & Platt, 2011; Lloyd-Evans 2016, Langdon-Jones et al., 2015, Pendin et al., 2015) will also prove invaluable.

Aquaculture, of both freshwater and marine fish is a major growth industry worldwide, and provides a crucial source of animal protein production (Buchmann, 2013). Elimination of parasitic infections from fish farms, a concerning cause of lost productivity presents a continuing challenge requiring new measures, especially since the ban on the use of nitroimidazole control agents *e.g.*, metronidazole (Millet et al., 2010, 2013a). Understanding of the unique features of the basic biochemistry and immunology of diplomonad infectivity presents new opportunities for reduction of morbidity and mortality of farmed fish.

In summary, this study reveals gross surface and internal structural characteristics of *S. vortens,* not readily visualized in situations where an electron microscope or molecular methods are unavailable, but also essential for definitive identification of harmful parasites and closely related species. Control of fish infections by diplomonad parasites presents continuing problems in an expanding industry, and implementation of new measures requires specific diagnoses for control and management (Buchmann et al., 1995; Williams, 2013, Williams et al., 2015).

The methods used here reveals that calcium binding sites are generally distributed throughout this organism, but are most prominently localized in hydrogenosomes, as observed previously for a trichomonad, a rumen fungus and a sediment dwelling ciliate, thereby retaining the property of calcium storage in mitochondria, their evolutionary ancestors. Dynamic measurements of physiological processes in *S. vortens* using calcium fluorophores requires anaesthetized organisms as previously described (Langdon-Jones et al., 2015). Super-resolution imaging will in future enable new insights into structure-function relationships, not only in the cells of higher organisms and eukaryotic microbes (Ranjbari et al., 2019), but also in prokaryotes (Smitten et al., 2019).

Supplementary 1. A movie showing the rapid motility of *Spironucleus vortens* collected at 30 fps using an inverted fluorescence microscopy (XDY-2, 'GX Microscopes with cooLED Excitation Source').

Supplementary 2. *Spironucleus vortens* lightly anaesthetised to reveal slowed flagellar and intracellular organelle motility: paired nuclei, blue (DAPI) and hydrogenosomes red (CTC) using a Leica TCS SP2 AOBS confocal system.

Supplementary 3. Rotational aspects of *Spironucleus vortens* to reveal external surface morphology and arrangement of flagella as well as internal organelles as highlighted by binding of the Ca^{2+} fluorophore. These images were obtained by using a Zeiss LSM 880 upright confocal microscope (with Airyscan: a fast scanning super-resolution confocal system with fluorescence correlation spectroscopy (FCS) and fluorescence lifetime imaging (FLIM)).

Supplementary 4 (a) A movie through a z-stack of simultaneously acquired CARS (at 2850 cm^{-1}) and SHG images. The CARS highlights lipid droplets (red) within the *S. vortens*, while the SHG picks out the ordered structure of the flagella (blue). (b) A movie showing a 3D reconstruction of the z-stack in (a). The images were acquired using a home build CARS microscope based around a commercial Nikon Ti-U microscope Pope et al., 2013. Movies were generated using the Fiji bundle of ImageJ. Specifically the plugin 3D Viewer was used for the 3D reconstruction.

Acknowledgements

C. F. W holds a Sêr Cymru II Fellowship part-funded by the European Regional Development Fund through the Welsh Government. D. L is Hans

Christian Andersen Visiting Professor at the University of Southern Denmark, and is indebted to Dr. Peter Watson for Lipid TOX™ fluorophore, and E. Lloyd-Evans for fluors specifc for endoplasmic reticulum, lysosomes, and Golgi membranes. L. F. O. is supported by the Danish Council for Independent Research, Natural Sciences (DFF 4002- 00465).

The Zeiss LSM880 confocal microscope and Bitplane Imaris software were purchase through generous support of Cardiff University's Research Infrastructure Fund.

References

Amoroso, A. J. & Pope, S. J. (2015). Using lanthanide ions in molecular bioimaging. *Chemical Society Reviews 44 (14),* 4723-4742.

Amoroso, A. J., Coogan, M. P., Dunne, J. E., Fernández-Moreira, V., Hess, J. B., Hayes, A. J., Lloyd, D., Millet, C. Pope, S. J. & Williams, C. F. (2007). Rhenium *fac*-tricarbonyl bisimine complexes: biologically useful fluorochromes for cell imaging applications. *Chemical Communications (Cambridge) 7 (29),* 3066-3068.

Amoroso, A. J., Arthur, R. J., Coogan, M. P., Court, J., Fernández-Moreira, V., Hayes, A. J., Lloyd, D., Millet, C. Pope, S. J. (2008) 3-chloromethylpyrdyl biprridine fac-tricarbonyl rhenium: a new thiol-rective luminophore for fluorescence microscopy accumulates in mitochondria. *New Journal of Chemistry 32,* 1097-1102.

Andrews, M., Jones, J. E., Harding, L. P. & Pope, S. J. A. (2011). Luminescent probes based on water-soluble, dual emissive lanthanide complexes: metal ion-induced modulation of near IR emission. *Chemical Communications, 2011, 47*, 206-208.

Balasingham, R. G., Coogan, M. P. & Thorp-Greenwood, F. L. (2011) Complexes in context: attempting to control the cellular uptake and localiisation of rhenium *fac*-tricarbonyl polypyridyl complexes. *Dalton Transactions 40 (44),* 11663-11674.

Balasingham, R. G., Thorp-Greenwood, F. L. Williams, C. F. Coogan, M. P. & Pope, S. J. (2012). Biologically compatible, phosphorescent dimetallic rhenium complexes linked through functionalized alkyl chains: syntheses, spectroscopic properties, and applications in imaging microscopy. *Inorganic Chemistry 51 (3),* 1319-1426.

Biagini, G. A., Finlay, B. J. & Lloyd, D. (1997a). Evolution of the hydrogenosome. *FEMS Microbiology Letters 155*, 133-140.

Biagini, G. A., Suller, M. T. E., Finlay, B. J. & Lloyd, D. (1997b). Oxygen uptake and antioxidant responses of the free-living diplomonad *Hexamita* sp. *Journal of Eukaryotic Microbiology 44*, 447–53.

Biagini, G. A. vanderGiezen, M., Hill, B., Winters, C. & Lloyd, D. (1997c). Ca^{2+} accumulation in the hydrogenosomes of *Neocallimastix frontalis* L2 a mitochondrial-like physiological role.*FEMS Microbiology Letters 149*, 227-232.

Biagini, G. A., Hayes, A. J., Suller, M. T. E., Winters, C., Finlay, B. J. & Lloyd, D. (1997d). Hydrogenosomes of *Metopus contortus* physiologically resemble mitochondria. *Microbiology* 143**,** 1623-1629.

Biagini, G.A., Yarlett, N., Ball, G. E., Billetz, A. C., Lindmark, D. G., Martinez, M. P., Lloyd. D. & Edwards, M. R. (2003). Bacteria-like energy metabolism in the amitochondriate protozoon, *Hexamita inflata. Molecular and Biochemical Parasitology 128(1),* 11-19.

Bradley, J. Pope, I., Masia, F., Sanusi, R., Langbein, W., Swann, K. & Borri, P. (2016). Quantitative imaging of lipids in live mouse oocytes and early embryos using CARS microscopy. *Development, 143, (12),* 2238-2247.

Bradley, J. Pope, I., Wang, Y., Langbein, W., Borri, P. & Swann, K. (2019). Dynamic label-free imaging of lipid droplets and their link to fatty acid and pyruvate oxidation in mouse eggs. *Journal of Cell Science 132(13),*

Brugerolle, G., Kunstyr, I., Senaud, & J. Friedhof, K.T. (1980) Fine structure of trophozoites and cysts of the pathogenic diplomonad, *Spironucleus muris. Zeitschrift für Parasitenkunde 62(1),* 47-61.

Buchmann, K. (2013). Impact and control of protozoan parasites in maricultured fishes. *Parasitology 142*, 168-177.

Buchmann, K., Uidaal, A. & Lyholt, H. C. (1995). Parasite infections in Danish trout farms. *Acta Veterinaria Scandinavica 36(3),* 283- 298.

Cammack, R., Horner, D. S., van der Giezen, M., Kulda, J. & Lloyd, D. (2003). Iron-sulphur in anaerobic eukaryotes. In: L. Ljungdahl, M. W. W. Adams, L. L. Barton, J.G. Ferry & M. K. Johnson (Eds.) *Physiology and Biochemistry of Anaerobic Bacteria* (pp.113-127), New York: Springer.

Campbell, A. K. (2017). *Fundamentals of Intracellular Calcium*. Chichester: Wiley:

Carafoli, E. & Krebs, J. (2016). Why calcium ? How calcium became the best communicator. *Journal of Biological Chemistry 291(40)*, 20849- 20857.

Carafoli, E., Lehninger, A. L. (1971). A survey of the interactions of

Calcium ions with different tissues and species. *Biochemical Journal 122*, 681-690.

Carafoli, E., Balcavage W, X., Lehninger, A. L., Mattoon, J. R. (1970).

Ca^{2+} metabolism in yeast cells and mitochondria. *Biochimica*

*Biophysica Acta 205,*18- 26.

Chance, B., Schoener, B. & Elsaesser, S. (1966). Metabolic control phenomena involved in damped sinusoidal oscillations of reduced diphosphopyridine nucleotide in a cell-free extract of *Saccharomyces carlsbergensis. Journal of Biological Sciences 240,* 3170-3181.

Chapman, A., Hann, A.O., Linstead D & Lloyd, D. (1986a). Dispersive X-ray microanalysis of membrane associated inclusions in hydrogenosomes isolated from *Trichomonas vaginalis. Journal of General Microbiology 131*, 2933-2939.

Chapman, A., Cammack, R., Linstead, D. & Lloyd, D. (1986b). Respiration of *Trichomonas vaginalis*. Components detected by electron paramagnetic resonance spectroscopy. *European Journal of Biochemistry 156*, 193-198.

Coogan, M. P, Fernández-Moreira, V., Kariuki, B. M., Pope, S. J. A. & Thorp-Greenwood, F., L. (2009). A rhenium tricarbonyl 4'-oxo-terpy trimer as a luminescent molecular vessel with a removable silver stopper. *Angewandt Chemie International Edition, 48,* 4965-4968.

Coogan, M. P, Court, J. B., Gray, V. L., Hayes, M. J., Lloyd, S. H., Millet, C. O., Pope, S. J. & Lloyd, D. (2010) Probing intracellular oxygen by quenched phosphorescent lifetimes of nanoparticles containing polyacrylamide-embedded [$Ru(dpp(SO_3Na_2)_3)$]Cl_2. *Photochemical Photobiological Sciences 9 (1),* 103-109.

Coogan M.P. & Fernández-Moreira, V. (2014). Progress with and prospects for metal complexes in cell imaging. *Chemical Communications 50*, 384-399.

Denikina, N., Nebesnykh, I., Maikova, O., Dzyuba, E. & Belkova, N. (2016).Genetic diversity of Diplomonadida in fish of the genus Coregonus from Southeastern Siberia. *Acta Parasitologica. 61*, 299-306.

Denikina, N. N., Nebesnykh, I. A., Kondratova, L. G., Khanaev, I. V. & Dzyuba, E. V. (2018). Representatives of Diplomonadida in fishes of East Siberia. *Limnology and freshwater biology 2,* 106

Denikina, N. N., Kondratov, I., Belkova, N. & Sokalov, S. (2019). The phylogenetic position of *Spironucleus* sp. (Diplomonadida: Hexamitidae) from the intestine of Chinese Sleeper *Perccottus glenii* Dybowski, 1877 (Actinopterygii: Odontobutidae). *Acta Parasitologica 64(2),*347-351.

Di Napoli, C., Masia, F., Pope, I., Otto, C., Langbein, W. & Borri, P. (2014a). Chemically-specific dual/differential CARS micro-spectroscopy of saturated and unsaturated lipid droplets. *Journal of Biophotonics 7,* 68-76.

Di Napoli, C., Pope, I, Masia, F., Watson, P., Langbein, W. & Borri, P. (2014b). Hyperspectral and differential CARS microscopy for quantitative chemical imaging in human adipocytes. *Biomedical Optical Express 5(5),* 1378-1390.

Di Napoli, C., Pope, I, Masia, F., Langbein, W. Watson, P., & Borri, P. (2016). Quantitative spatiotemporal chemical profiling of individual lipid droplets by hyperspectral CARS microscopy in living 3677-3685 human adipose–derived stem cells. *Analytical Chemistry 88(7),* 3677-3685.

Docampo, R., Jimenez, V., Lander, N., Li, Z. H. & Niyoji, S. (2013). New insights into roles of acidocalcisomes and contractile vacuole complex in protists. *International Reviews of Cellular and Molecular Biology 305*, 69-113.

Deorner, J. F., Delling, M. & Clapham, D.E. (2015). Ion channels and calcium signaling in motile cells. *Elife 4*, e11066.

Eliseeva, S. V. & Bunzli, J. C. G. (2010) Lanthanide luminescence for functional materials and biosciences. *Chemical Society Reviews 39*, 189-227.

Ellis, J. E., McIntyre, P. S., Saleh, M., Williams, A. G. & Lloyd, D. (1991). The influence of ruminal concentrations of O_2 on fermentative metabolism of the rumen entodiniomorphid ciliate, *Eudiplodinium maggii. Current Microbiology 23,* 245-251.

Evans, W. H. (2006). Cell communication across gap junctions: ahistorical perspective and current developments. *Biochemical Society Transactions 43 (3)*, 450-459.

Fard, M. R. S., Jørgensen, A., Sterud, E., Bleiss, W. & Poynton, S. L. (2007). Ultrastructure and molecular diagnosis of *Spironucleus salmonis* (Diplomonadida) from rainbow trout *Oncorhynchus mykiss* in Germany. *Diseases of Aquatic Organisms 75,* 37-50.

Faulkner, S., Pope, S. J. A., & Burton-Pye, B. P. (2005) Lanthanide complexes in the luminescence imaging applications. *Applied Spectroscopy Reviews 40,* 1-31.

Felton, C. E., Harding, L, P., Jones, J. E, Kariuki, B. M., Pope, S. J. A. & Rice, C.R. (2008) A wavelength and lifetime responsive cryptate-containing fluorescent probe for zinc ions in water. *Chemical Communications, 2008*, 6185-6187.

Fernández-Moreira, V., Thorp-Greenwood & Coogan, M. P. (2010a). Application of d6 transition metal complexes in fluorescence cell imaging. *Chemical Communications (Camb.) 46(10),* 186-202.

Fernández-Moreira, V., Thorp-Greenwood, F. L., Amoroso, A. J., Cable, Court, J. B., Gray, V. L., Hayes, M. J., Jenkins, R. L., Kariuki, B. M., Lloyd, D., Millet, C. O., Williams, C. F. & Coogan, M. P. (2010b). Uptake and localization of rhenium fac-tricarbonyl polypyridyls in fluorescent cell imaging experiments. *Organic and Biomolecular Chemistry 8 (17),* 3888-3901.

Gerasimenko, J. V., Tepikin, A. V. Petersen, O. H. & Gerasimenko, O. V. (1998). Calcium uptake via endocytosis with rapid release from acidifying endosomes. *Current Biology 8,* 1335-1338.

Gerencśer, A. A. & Adam-Visi, V. (2001). Selective high-resolution fluorescence imaging of mitochondrial Ca^{2+} concentration. *Cell Calcium 30,* 311-321.

Gerencśer, A. A. & Adam-Visi, V. (2005). Mitochondrial Ca^{2+} dynamics reveals limited intra-mitochondrial Ca^{2+} diffusion. *Biophysical Journal 88,* 698-714.

Gerencśer, A. A., Chinopoulos, C., Birket M. J., Jastroch, M., Vitelli, C., Nicholls, D. G. & Bränd, M. D. (2012). Quantitative measurement of mitochondrial membrane potential in cultured cells: calcium-induced de- and hyperpolarisation of neuronal mitochondria. *Journal of Physiology 590,* 2845-2871.

Gerencśer, A. A., Mulder, H. & Nicholls, D. G. (2017). Calcium modulation of exocytosis-linked plasma membrane potential oscillations in INS-1 832/13 cells. *Biochemical Journal 471,* 111-122.

Groves, L. M., Williams, C. F., Hayes, M. J., Ward, B. D., Isaacs, M. D., Symonds, N. O., Lloyd, D., Horton, P. N., Coles, S. J., Pope, S. J. A. (2019). *Dalton Transactions 48 (5)*, 1599-1612.

Häder, D. P. & Hemmersbach, R. (2017). Gravitaxis in *Euglena*. *Advances in Experimental Medicine and. Biology, 979,* 237- 266.

Hallett, A. J., Placet, E., Prieux, R., McCafferty, D. M., Platts, J. M. Lloyd, D., Isaacs, M., Hayes, A. J., Coles, S. J., Pitak, M. P., Marchant, S., Marriott, Allemann, R., K., Dervisi, A. & Fallis, I. A. (2018). Exploring the cellular uptake and localization of phosphorescent rhenium *fac*-tricarbonyl metallosurfactants as a function of lipophilicity. *Dalton Transactions 47 (40),* 14241-14253.

Hallett, A. J., Christian, P., Jones, J. E. & Pope, S. J. A. (2009). Luminescent, water soluble gold nanoparticles functionalized with ^{3}MLCT emitting rhenium complexes. Chemical Communications 4278-4280.

Horner, D. S., Hirt, R. P., Kilvington, S., Lloyd, D. & Embley, T. M. (1996). Molecular data suggest an early acquisition of the mitochondrion endosymbiont. *Proceedings of the Royal Society-biological sciences, 263,* 1053-1059.

Humphreys, M. Ralphs, J., Durrant, L., & Lloyd, D. (1994). Hydrogenosomes in trichomonads are Ca^{2+} stores and have a transmembrane electrochemical potential. *Biochemical Society Transactions 22,* 324S.

Humphreys, M., Ralphs, J., Durrant, L. & Lloyd, D. (1998). Confocal laser scanning microscopy of trichomonads: hydrogenosomes store calcium and show a membrane potential. *European Journal of Protistolology 34,* 356-362.

Jerlström-Hultqvist, J., Einarsson, E., Xu, F., Hjort, K., Ek, B., et al. (2013). Hydrogenosomes in the diplomonad *Spironucleus salmonicida*. *Nature Communications 4,* 2493.

Jørgensen, A. & Sterud, E. (2006) The marine pathogenic genotype of *Spironucleus barkhanus* from farmed salmon redescribed as *Spironucleus salmonicida* n. Sp. *Journal of Eukaryotic Microbiology 53,* 531-541.

Jørgensen, A., Torp, K., Bjørland, M.A., & Poppe, T. T. (2011). Wild arctic char Salvelinus alpinus and trout Salmo trutta: hosts and reservoir of the

salmonid pathogen *Spironucleus salmonicida* (Diplomonadida; Hexamitidae). *Diseases of Aquatic Organisms 97,* 57-63.

Jones, J. E. & Pope, S. J. A. (2009) Sensitised near-IR lanthanide luminescence exploiting anthraquinone-derived chromophores: syntheses and spectroscopic properties. *Dalton Transactions 2009*, 8421-8425.

Jones, J. E. Jenkins, R. L. Hicks, R. S., Hallett, A. J. & Pope, S. J. (2012). Water soluble, luminescent iridium(III)-ytterbium(III) complexes using dipyrido[3,2-a:2' 3'-c]phenazine as bridging units. *Dalton Transactions 41,* 10372-19381. 10.1039/c2dt31115a

Jones, J. E., Amoroso, A. J., Dorin, I. M., Parigi, G., Ward, B. D., Buurma, N. J. & Pope, S. J. A. (2011). Bimodal, dimetallic lanthanide complexes that bind to DNA: the nature of binding and its influence on water activity. *Chemical Communications, 47,* 3374-3376.

Langdon-Jones, E. E., Symonds, N. O., Yates, S. E., Hayes, A. J., Lloyd, D., Williams, R., Coles, S. J, Horton, P. N. & Pope, S. J. (2014). Fluorescent rhenium-naphthalimide conjugates as cellular imaging agents. *Inorganic Chemistry 53 (7),* 3788-3797.

Langdon-Jones, E. E., Lloyd, D., Hayes, A. J., Wainwright, S. D. Mottram, H. J., Coles, S.J., Horton, P. N. & Pope, S. J. (2015). Alkynyl-naphthalimide fluorophores: gold coordination chemistry and imaging applications. *Inorganic Chemistry 54 (13),* 6606-6615.

Langdon-Jones, E. E., Jones, A.B., Williams, C. F., Hayes, A. J., Lloyd, D., Mottram, H. J., Groves, L. M. & Pope, S. J. A. (2017a). Anticancer, azonafide-inspired fluorescent ligands and their rhenium(I) complexes for cellular imaging. *European Journal of Inorganic Chemistry 2017* (3), 759-766.

Langdon-Jones, E. E., Jones, A. B., Williams, C. F., Hayes, A. J., Lloyd, Coles, S. J, Horton, P. N. Groves, L. M. & Pope, S. J. (2017b). Luminescent 1, 8-naphthalamide-derived Re^{I} complexes: syntheses, spectroscopy, X-ray structure and preliminary bioimaging in yeast cells. *European Journal of Inorganic Chemistry*, 5279-5287.

Lantsman, Y., Tan, K. S., Morada, M. & Yarlett, N. (2008). Biochemical characterization of a mitochondrial-like organelle from *Blastocystis* sp. subtype 7. *Microbiology 154,* 2757-2766.

Leitsch, D., Williams, C. F. & Hrdy, I. (2018). Redox pathways as drug targets in microaerophilic parasites. Trends in Microbiology 34(7), 576-589.

Li, L.Z., Xu, H.N., Rangi, M., Nioka, S., Chance, B. (2009). Mitochondrial redox imaging for cancer diagnostic and therapeutic studies. *Journal of Innovative Optical Health Sciences, 2 (4),* 325-341.

Lindmark, D. G. & Muller, M. (1973). Hydrogenosome, a cytoplasmic organelle of the anaerobic flagellate *Tritrichomonas foetus*, and its role in pyruvate metabolism. *Journal of Biological Chemistry 248,* 7724-7728.

Liu, R., Guan, Y., Chen, L. & Lian, B. (2018). Adsorption and desorption characteristics of Cd^{2+} and Pb^{2+} by micro and nano-sized biogenic $CaCO_3$. *Frontiers in Microbiology 9,* 41.

Lloyd, D. (1974). *The Mitochondria of Microorganisms*, pp. 103-104, London: Academic Press.

Lloyd, D. (2002). Non-invasive methods and the investigation of organisms in low O_2 levels. In G. M. Gadd, (Ed.), *Advances in Applied Microbiology 51,* 155-183.

Lloyd, D. & Williams, A. G. (1993). Biological activities of symbiotic and parasitic protists in low O_2 environments. In J. G. Jones, (Ed.), *Advances in Microbial Ecology 13,* (pp. 211-262). New York: Plenum Press.

Lloyd, D. & Williams, C. F. (2014). Comparative biochemistry of Giardia, Hexamita and Spironucleus: enigmatic diplomonads. *Molecular and Biochemical Parasitology 197 (1-2),* 43-49.

Lloyd, D. & Williams, C. F. (2015). Avoid excessive oxygen in experiments with organisms, tissues and cells. *Advances in Microbial Physiology 67*, 293-314.

Lloyd, D., Ralphs, J. R. & Harris, J. C. (2002). *Giardia intestinalis*, a eukaryote without hydrogenosomes, produces hydrogen. *Microbiology 148,* 727-733.

Lloyd, D., Coogan, M. P. & Pope, S. J. (2012). Novel metal-based luminophores for biological imaging. In Geddes, C. D. (ed.) *Reviews in Fluorescence* 2010*, Vol. 7.*, Springer Science + Business Media, LLC pp. 15-44.

Lloyd, D., Ellis, J. D., Hillman, K. D. & Williams, A. G. (1993). Membrane inlet mass spectrometry: probing the rumen ecosystem. *Journal of Applied Bacteriology Symposium Supplement 73,* 155-163.

Lloyd, D., Moran, C., Suller, M. T. E. & Dinsdale, M. G. (1996) Flow cytometric monitoring of rhodamine 123 and cyanine dye uptake by yeast during cider fermentation. *Journal of the Institute of Brewing 102,* 251-259.

Lloyd, D., Williams, C. F., Vijayalakshmi, E., Kombrabail, M, White, N., Hayes, A. J., Aon, M. A. & Krishnamoorthy, G. (2014) Intracellular oxygen: similar results from two methods of measurement using phosphorescent nanoparticles. *Journal of Innovative Optical Health Sciences 7 (2),* 1350041.

Lloyd, D., Lewis, I. B., Williams, C. F., Hayes, A. J., Symons, H. & Hill, E. C. (2015). Motility of the diplomonad fish parasite *Spironucleus vortens* through thixotropic solid media. *Microbiology 161 (1),* 213-218.

Lloyd, D., Murray, D. B., Aon, M. A., Cortassa, S., Roussel, M. R., Beckmann, M. & Poole, R. K. (2018). Temporal metabolic partitioning of the yeast and protist cellular networks: the cell is a global scale-invariant (fractal or self-similar) multioscillator. *Journal of Biomedical Optics, 24* (5), 051404.

Lloyd-Evans, E. & Platt, F.M. (2011). Lysosomal Ca^{2+} homeostasis: role in pathogenesis of lysosomal storage diseases. *Cell Calcium 50,* 200-205.

Lloyd-Evans, E. (2016). On the move, lysosomal CAX drives Ca^{2+} transport and motility. *Journal of Cell Biol*ogy 212, 755-757.

Lo, K. K., Louie, M., Sze, K. & Lau, J. (2008a). Rhenium (I) polypyridyl biotin isothiocyanate complexes as the first luminescent tiotinylation reagents: synthesis, photophysical properties, biological labelling, cytotoxicity and imaging studies. *Inorganic Chemistry 47*, 602-611.

Lo, K. K., Le, T. K. M., Lo, J. S. Y., Poon, W. L. & Cheng, S. H. (2008b). Luminescent biological probes derived from ruthenium (II) complexes. *Inorganic Chemistry 47,* 200-2008.

McDonald, T. F., Pelzer, S., Trautwein, W. & Pelzer, D. J. (1994). Regulation and modulation of calcium channels in cardiac, skeletal and smooth muscle cells. *Physiological Reviews 74,* 365-507.

Millet, C. O. M. (2010). Growth, metabolism, ultrastructure and chemotherapy of *Spironucleus vortens*. PhD Thesis, Cardiff University, Wales.

Millet, C. O. M., Cable, J. & Lloyd, D. (2010). The diplomonad fish parasite *Spironucleus vortens* produces hydrogen. *Journal of Eukaryotic Microbiology 57,* 400 – 405.

Millet, C. O. M., Lloyd, Williams, C.F. & Cable, J. (2010a). *In vitro* culture of the diplomonad fish parasite *Spironucleus vortens* reveals unusually fast doubling times and atypical biphasic growth. *Journal of Fish Diseases, 34 (1),* 71-73.

Millet, C. O. M., Lloyd, D., Williams, C. F., Williams, D., Evans, G. Saunders, R. A. & Cable, J. (2010b). Effect of garlic and allium-derived products on

the growth and metabolism of *Spironucleus vortens. Experimental Parasitology 127*, 490-499.

Millet, C. O., Lloyd, D., Coogan, M. P., Rumsey, J. & Cable, J (2011). Carbohydrate and amino acid metabolism of *Spironucleus vortens*. *Experimental Parasitolology 129,* 17–26.

Millet, C. O., Lloyd, D., Williams, C. F., Hayes, A. J., Hann, A.C. & Cable J. (2013). Mitochondria-derived organelles in the diplomonad fish parasite *Spironucleus vortens. Experimental Parasitology 135,* 262–273.

New, E. J. & Parker, D. (2009). The mechanism of cell uptake for luminescent lanthanide optical probes: the role of micropinocytosis and the effect of enhanced membrane permeability on compartmentalisation *Organic and Biomolecular Chemistry 7(5),* 851- 855.

Omelon, S., Ariganello, M., Bonucci, E., Grynpas, M. & Nanci, A. (2013). A review of phosphate mineral nucleation in biology and geobiology. *Calcification of Tissue International 93,* 382-96.

Paul, R. G., Williams, A. G. & Butler, R. D. (1990). Hydrogenosomes in the rumen entodiniomorphid ciliate *Polyplastron multivesiculatum*. *Journal of General Microbiology136,* 1981-1989.

Paull, G. C. & Matthews, R. A. (2001). *Spironucleus vortens*, a possible cause of hole-in-the-head disease in cichlids. *Diseases of Aquatic Organisms 45*, 197-202.

Pendin, D., Greotti, E., Filadi, R. & Pozzan, T. (2015). Spying on organelle Ca^{2+} in lving cells: the mitochondrial point of view. *Journal of Endocrinology Investigation 38* , 39-45.

Pope, I., Langbein, W., Watson, P. & Borri, P. (2013) Simultaneous hyperspectral differential CARS, TPF and SHG microscopy with a single 5fs Ti:Sa laser. *Optical Express 21*, 7096-7106.

Poynton, S.L. & Morrison, C. M. (1990). Morphology of diplomonad flagellates *Spironucleus torosa* n. sp. from Atlantic cod (*Gadus morhua hua* L., and haddock *Melanogrammus aelglefinus* L., and *Hexamita salmonis* Moore from brook trout *Salvelinus fontinalis* (Mitchill). *Journal of Protozoology 37*, 369-383.

Poynton, S. L., Fraser, W., Francis-Floyd, R., Rutledge, P., Reed, P. et al. (1995). *Spironucleus vortens* n. sp. from the fresh-water Angelfish *Pterophyllum scalare*: morphology and culture. *Journal of Eukaryotic Microbiology 42*, 731-742.

Poynton, S. L. & Sterud, E. (2002). Guidelines for species description of diplomonad flagellates in fish. *Journal of Fish Diseases 25*, 15-31.

Poynton, S. L., Fard, M. R., Jenkins, J. & Ferguson, H. W. (2004). Ultrastructure of *Spironucleus salmonis* n. com (*Octomitus salmonis*, sensu Moore 1922, Davis 1926, and *Hexamita salmonis* sensu Ferguson 1979), with a guide to spironucleus species. *Diseases of Aquatic Organisms 60,* 49-64.

Pritchard, V. E., Thorp-Greenwood, F. L. Balasingham, R., Williams, C. F., Kariuki, B., Platts, J. A., Hallett, A. J., & Coogan, M. P. (2013) Simple polyphenol zirconium and hafnium metallocene room-temperature lumophores for cell imaging. *Organometallics 32 (12),* 3566-3569.

Ranjbari, E., Majdi, S. & Ewing, A. (2019). Analytical techniques; shedding light upon nanometer-sized secretory vesicles. *Trends in Chemistry xx (x),xxx-xxx.*

Roxström-Lindquist, K., Jerlström-Hultquist, J., Jørgensen, A., Troell, K., Svärd, S. G. & Anderson, J. O. (2010). Large genomic differences between the Morphologically indistinguishable diplomonads, *Spironucleus barkhanus* and *Spironucleus salmonicida*. *BMC Genomics 11*, 258.

Senatore, A., Raiss, H. & Le, P. (2016). Physiology and evolution of voltage-gated calcium channels in early-diverging phyla: Cnidaria, Placozoa, Porifera and Ctenophora. *Frontiers of Physiology 4,* 481.e Collection 2016.

Smitten, K. L., Southam, H. M., Bernardino de la Serna, J., Gill, M. R., Jarman, P. J., Smythe, C. G. W., Poole, R. K. & Thomas, J. A. (2019). Using nanoscopy to probe the biological activity of antimicrobial leads that display potent activity against pathogenic, multidrug resistant, Gram-negative bacteria. *ACS Nano 13*, 5133-5145.

Stacey, O. J., Amoroso, A. J., Platts, J. A., Horton, P. N., Coles, S. J. Lloyd, D., Williams, C. F., Hayes, A. J., Dunsford, J. J. & Pope, S. J. A. (2015). Water soluble Cyclometalated Pt(II)-Ln(II) conjugates towards novel bimodal imaging agents. *Chemical Communications 51* (61), 12305-12308.

Stairs, C.W., Kokla, A., *Á*stvaldsson, *Á*, Jerlström-Hultqvist, J., Sv*ä*rd, S. & Etterna, T. J. G. (2019) Oxygen induces the expression of invasion and stress responce genes in the anaerobic salmon parasite *Spironucleus salmonicida. BMC Biology* 17(1), 19.

Sterud, E. (1998). Electron microscopical identification of the flagellate *Spironucleus torosa* (Hexamitidae) from burbot Lota lota (Gadidae) with comments upon its probable introduction to this freshwater host. *Journal of Parasitology 84(5),* 947-953.

Sterud, E. & Poynton, S. L. (1998). *Spironucleus vortens* (Diplomonadida) in the Ide, *Leciscus idus* (L.) (Cyprinidae): a warm water hexamitid flagellate found in Northern Europe. *Journal of Eukaryotic Microbiology 49 (2),* 137-145.

Sterud, E., Mo, T. A. & Poppe, T. (1997). Ultrastructure of *Spironucleus barkhanus* n. sp. (Diplomonadida: Hexamitidae) from grayling *Thymallus thymallus* (L.) (Salmonidae) and Atlantic salmon *Salmon salar* L. (Salmonidae). *Journal of Eukaryotic Microbiology 44,* 499-407.

Sterud, E., Mo, T. A. & Poppe, T. (1998). Systemic spironucleosis in sea-farmed Atlantic salmon *Salmo salar*, caused by *Spironucleus barkhanus* transmitted from feral Artic char *Salvelinus alpinus*. *Diseases of Aquatic Organisms 33,* 63-66.

Steel, H. L., Allinson, S. L., Andre, J., Coogan, M. P. & Platts, J. A. (2015) Platinum trimethyl bipyridyl thiolates- new tunable red- to near IR emitting luminophores for bioimaging applications. *Chemical Communications 51(57),* 11441-11444.

Stockert, J. C., Horobin, R. W., Colombo, L. L., Blázquez-Castro, A. (2018). Tetrazolium salts and formazan products in cell biology: viability assessment, fluorescence imaging and labeling perspectives. Acta Histochemica 120(3), 159-167.

Thorp-Greenwood, F., L., Fernández-Moreira, V., Millet, C. O., Williams, C. F., Cable, J., Court, J. B., Hayes, A. J., Lloyd, D. & Coogan, M. P. (2011) A 'Sleeping Trojan Horse' which transports metal ions into cells, localises in nucleoli and has potential for bimodal fluorescence/PET imaging. Chemical Communications 47 (11), 3096-3098.

Thorp-Greenwood, F., L., Coogan, M. P., Mishra, L., Kumari, N., Rai, G. & Srikrishna, S. (2012). The importance of cellular localization of probes: synthesis, photophysical properties, DNA interactions and cellular imaging properties of rhenium dppz complexes with known cellular localization vectors. *New Journal of Chemistry 36,* 64-72.

Tovar, J., Leon-Avila, G., Sanchez, L. B., Sutak, R., Tachezy, J., van der Giezen, M., Hernandez, M., Muller, M. & Lecocq, J.M. (2003). Mitochondrial remnant organelles of Giardia function in iron-sulphur protein maturation. *Nature 426,* 172-176.

Weiland, M. E., McArthur, A. G., Morrison, H. G., Sogin, & M. L. Svärd, S. G. (2005). Annexin-like alpha-giardins: a new cytoskeletal gene family in *Giardia lamblia. International Journal of Parasitology 35*, 617-626.

Wenman, W. M., Meuser, R. U., Nyugen, Q., Kilani, R. T., eL-Shewy, K. & Sherburne, R. (1993). Characterisation of an immunodominant *Giardia lamblia* annexin related to alpha giardin. *Parasitology Research 79*, 587-592.

Williams, C. F. (2013) Life cycle, biochemistry, and chemotherapy of *Spironucleus vortens*. PhD Thesis, Cardiff University, Wales.

Williams, C. F., Lloyd, D., Poynton S. L., Jørgensen, A., Millet, C. O. M. & Cable, J. (2011). *Spironucleus* species: economically important fish pathogens and enigmatic single-celled eukaryotes. *Journal of Aquaculture Research and Development* s2, http//dx.doi.org/10.4172/2155-9546.S2- 00.

Williams, C.F., Lloyd, D., Kolarich, D., Alagesan, K., Duchene, M, Cable, J., Williams, D. & Leitsch, D. (2012a). Disrupted intracellular redox balance of the diplomonad fish parasite Spironucleus vortens by 5-nitroimidazole and garlic-derived compounds. *Veterinary Parasitology 190 (1-2),* 62-73.

Williams, C.F., Kombrabail, M, Vijayalakshmi, K., White, N., Krishnamoorthy, G. & Lloyd, D. (2012b) Evaluation of two novel methods of measurement of intracellular oxygen. *Measurement Science and Technology 23 (8)*, 084005.

Williams, C. F., Millet, C. O. M., Hayes, A. J., Cable, J. & Lloyd, D. (2013a). Diversity in mitochondrion- derived organelles of the parasitic diplomonads *Spironucleus* and *Giardia*. *Trends in Parasitology 29*, 311–2.

Williams, C. F., Vacca, A. R., Lloyd, D., Schelkle, B., & Cable, J. (2013b). Non-invasive investigation of *Spironucleus vortens* transmission in freshwater angelfish *Pterophyllum scalare*. *Diseases of Aquatic Organisms 105*, 211-223.

Williams, C. F., Yarlett, N., Aon, M. A. & Lloyd, D., (2014).

Antioxidant defences of *Spironucleus vortens*: Glutathione is the major non-protein thiol. *Molecular and Biochemical Parasitology 196(1),* 45-52.

Wolinski, H., Natter, K. and Kohlwein, S. D. (2009). The fidgety yeast: focus on high- resolution live yeast cell microscopy. *Methods in Molecular Biology 548,* 75-99.

Wolinski, H., Kolb, D., Hermann, S., Koning, R.I. & Kohlwein, S. D. A role for seipin in lipid droplet dynamics and inheritance in yeast.in (2011) Journal of Cell Science 124, 3894-3904.

Woo, P. T. K. & Poynton, S. L. (1995) Diplomonadida, Kinetoplastida and Amoebaida (Phylum Sarcomastigophora) In Fish Diseases and disorders, Vol. 1. Protozoan and Metazoan Infections, pp. 27-96. P. T. K. Woo (ed.)
Wallingford UK: CAB International.

Xu, H. N., Tchou, J, Chance, B. & Li, L. Z. (2013). Imaging the redox states of human breast cancer core biopsies. *Advances in Experimental Medical Biology, 765,* 343-349.

Yarlett, N., Hann A. C., Lloyd, D. & Williams, A. G. (1981). Hydrogenosomes in the rumen protozoon *Dasytricha ruminantium* Schuberg. *Biochemical Journal 200 (2),* 365-372.

Yarlett N., Orpin C. G., Munn, E. A., Yarlett, N. C. & Greenwood C. A. (1986). Hydrogenosomes in the rumen fungus, *Neocallimastix patriciarum. Biochemical Journal 236 (3),* 729-739.

Yarlett, N., Lindmark, D. G., Goldberg, B, Moharrami, M. A. & Bacchi, C. J. (1994). Subcellular localization of the enzymes of the arginine dihydrolase pathway in *Trichomonas vaginalis* and *Tritrichomonas foetus. Journal of Eukaryotic Microbiology 41,* 554-559.

Yu, M., Zhao, Q., Shi, L., Li, F., Zhou, Z., Yang, H., Yi, T. & Huang, C. (2008). Cationic iridium (III) complexes for phosphorescence staining in the cytoplasm of living cells. *Chemical Communications 18,* 2115-2117.

Figure captions

Fig. 1. Jablonski diagram for transitions involved in Fluorescence and phosphorescence.

Fig. 2.Comparison of the autofluorescence spectra (λ_{ex} 458nm) of bright spherical inclusions in *S. vortens* (Regions Of Interest 1, 2, and 3) (and background areas within and outside the cytosol (ROIs 4, 5 and 6) (Millet, 2010, Millet et al. 2013).

Fig. 3. Sampling after presentation of quantum dots to *S. vortens* after (a) 2 s, (b) 10 min and (c) 20 min of endocytosis. Each sample was fixed in 3% (v/v) formaldehyde solution immediately on collection. (Millet, 2010).

Fig. 4. Live cell fluorescence imaging of *S. vortens* using 2% (w/v) chloral hydrate solution to restrict motility and intracellular motion, and a reactive oxygen species scavenger (DABCO) to minimize photobleaching. (a) DAPI (DNA, RNA, in paired nuclei); (b) CTC: tetrazolium reduction product in hydrogenosomes (a fluorescent formazan); (c) Nomarski phase contrast transmission image; (d) overlay of a, b and c; (e) TMRE: tetramethyl rhodamine ethyl ester for $\Delta\varphi$, hydrogenosomal transmembrane electrochemical potential. (f). Lipid TOX™.

Fig. 5. Images of *S. vortens* incubated with Re-L^2 and TMRE showing (clockwise from top left): green fluorescence from Re-L^2 (λ_{ex} = 488nm; λ_{em} = 515nm); red fluorescence from TMRE (λ_{ex} = 543nm; λ_{em} = 600nm); overlaid images showing co-localisation; Normarski phase transmission image. (Langdon-Jones et al., 2014) .

Fig.6. Cultured Human MCF-7 cells (breast adenocarcinoma) incubated with $[HL^3]PF_6$(top) and $[AuCl(L^3)]$ (bottom). Representative superimposed images where yellow-orange signifies co-localisation (from left to right) with endoplasmic reticulum, Golgi and lysosomal specific fluorophores respectively. Note strong lysosomal co-localisation (Groves et al., 2019).

Fig. 7a. Top: Normalised emission spectra of selected complexes excited at 405 nm (recorded in aerated acetone. Bottom Time resolved measurements showing the comparative decay profiles for ligand $[HL^3]PF_6$ (red) and complex $[AuCl(L^3)]$ (blue) against the instrument response (green).

b. FLIM images of MCF-7 cells incubated with $[HL^3]PF_6$ (left), and $[AuCl(L^3)]$ (right) using pulsed excitation at 440nm.

Fitted parameters (left): τ_1 = 9.2 ns (77%), τ_2 = 3.4 ns (20%), τ_3 = 0.4ns (3%); (right): τ_1 = 11.0ns (68%). τ_2 = 3.9 ns (25%), τ_3 = 0.5ns (7%) (Groves et al., 2019).

Fig. 8. A simplified model for sensitized lanthanide luminescence, and energy-level diagram for am emissive chromophore-appended lanthanide complex sensitized via a ligand-centred triplet excited state (abs = absorbance, fluor = fluorescence, phos = phosphorescence, ISC=intersystem crossing , ET= energy transfer (Amoroso & Pope, 2015).

Fig. 9 Steady state emission spectra for Eu-L^b (10^{-5} M) in the presence o(clockwise from top left) of Cu^{II}, Zn^{II}, Hg^{II}, and Cd^{II}. Recorded in buffered water pH7.4 (Andrews et al., 2011).

Fig. 10. Fig. 10. Fluorescence microscopy of several lanthanide probes colocalised with corresponding commercially available probes to visualize specific sub-cellular localisations, Coogan & Fernández-Moreira, 2014.

Fig. 11. Two-photon excited laser scanning microscope images of nanoparticle encapsulated Ru-coordinate complex electroporated into *Spironucleus vortens*. The scale bar = 10µm (Lloyd et al., 2014).

Fig. 12. Steady state emission spectra for **Ln-L2** (black, Yb; grey, Nd; light grey, Er) measured in D2O using λ_{ex} = 450nm. Spectra offset for clarity, Jones and Pope (2009).

Fig. 13. Comparative luminescence decay profiles of [2-M] $^{n+}$ where M =K($_{I}$), Zn($_{II}$), Fe($_{III}$), Ca($_{II}$), Li($_{I}$). Inset: wavelength dependent lifetime decays of [2M $^{n+}$] in an ionic mixture. Data fits and residuals are omitted for clarity. Felton et al., (2008).

Fig. 14. Near-IR emission spectrum of [Ir-L^{8}-Yb](PF6) recorded in D_2O (λ_{ex} = 410nm). Inset corresponding lifetime decay at 980nm in D_2O.

Fig. 15. The fluorescence emission spectrum of *S. vortens* suspensions after preincubation with X-Rhod, 5F, AM are shown, together with effects of EDTA, Ca^{2+} channel inhibitors and Ca^{2+} addition

Fig. 16. Anaesthetised *S. vortens* after incubation in growth medium, after 1.5h preincubation with X-Rhod, 5F, AM, still showing slight flagellar movements, and calcium binding sites in numerous organelles and widely distributed small vacuoles.

Fig. 17. Surface-rendered 3D optical images of a pair of fixed and washed *Spironucleus vortens* generated from a z-plane section stack (mean section thickness 0.4µm), after uptake and de-esterification of X-Rhod 5F, AM for 1.5 h; then plus 1mM $CaCl_2$, followed by 1.0mM EDTA and fixation in 3% formaldehyde in PBS. This shows a group of organisms each with 6 lateral and 2 posterior flagella and the arrangement of the 16 flagella in a single organism about to divide, the latter organism was used to generate the data seen in Figure. Colour-coding (green) reveals the surface structure, and organelles (red) having the highest internal residual Ca^{2+} concentrations i.e., the smaller hydrogenosomes, and larger lipid droplets and more diffuse nuclear phospholipid-rich membranes.

Fig.18. An optical section Z-series captured upwards through a single organism after treatment as in Figure 17. The 8 sections were selected to display the insertion of the flagella into the ventral surface of the organism, and the more dorsally situated hydrogenosomes. The image has been intensity coded to highlight foci of intense fluorescent staining. Scale bar 10µm.

Fig.19 . As in Fig. 17. A single section through a group of organisms selected to show the closely packed organisation of internal membranes and organelles, hydrogenosomes, (H) lipid droplets (LD), nuclear membranes (NM), and

small vacuoles and diffuse cytoplasmic labeling of . Some released hydrogenosomes from damaged organisms are also present. Scale bar = 10µm.

Fig.20. CARS and SHG images were acquired using the experimental setup shown above: M, mirror; DM dichroic mirror; SP57 glass block; R reflecting prism; λ/2 half-wave plate; BE beam expander; PBS polarizing beam splitter; F filter; The side-view of the optics between the two indicated arrows show the beam height difference. Graph: typical spectra of the laser pump, Stokes, and TPF beams. (Pope, I. et al., (2013).

Fig. 21. (a). *S. vortens*: a CARS image (20 x 20 µm) taken at a vibrational resonance = 2830 cm^{-1} (scale bar =2µm): the yellow dashed line indicates the region where a hyperspectral line cut was taken. Stars indicate points from where spectra were taken. (b). The CARS line scan taken across the region of the yellow dashed line, in (a). The line covers the vibrational range from 2100 cm^{-1} to 4000 cm^{-1}, thereby extending beyond the filter range (2500 cm^{-1} to 3800 cm^{-1}), so that background levels can be determined. (c). The graph (left) shows the spectra averaged over the regions identified by the boxes in (b); The graph (right) shows the same data as in the graph to the left with the water spectrum (W, with a peak centred around 3270 cm^{-1}) subtracted. The spectrum L1 has a familiar lipid profile with a maximum at around 2840cm^{-1}.

Fig.22. The montage above shows a series of z-slices (0.5 µm apart) through the *S. vortens* centred in the image. Each individual image is 29 x 21 µm (289 x 210 pixels) and shows simultaneously acquired CARS at 2850 cm^{-1} (red) and SHG (blue). See Supplementary 4 for movies of the z-stack and 3D reconstruction.

Supplementary 1. A movie showing the rapid motility of *Spironucleus vortens* collected at 30 fps using light microscopy.

Supplementary 2. *Spironucleus vortens* lightly anaesthetised to reveal slowed flagellar and intracellular organelle motility: paired nuclei, blue (DAPI) and hydrogenosomes red (CTC). Images scanned on a Leica SP2 AOBS confocal microscope.

Supplementary 3. Rotation of *Spironucleus vortens* to reveal external surface morphology and arrangement of flagella as well as internal organelles as highlighted by binding of the Ca^{2+} fluorophore.

Images scanned on a Zeiss LSM880 Airyscan confocal microscope. Surface rendering of organisms was using Bitplane Imaris software.

Supplementary 4 (a) A movie through a z-stack of simultaneously acquired CARS (at 2850 cm^{-1}) and SHG images. The CARS highlights lipid droplets (red) within the *S. vortens*, while the SHG picks out the ordered structure of the flagella (blue). (b) A movie showing a 3D reconstruction of the z-stack in (a). The images were acquired using a home build CARS microscope based around a commercial Nikon Ti-U microscope Pope et al., 2013. Movies were generated using the Fiji bundle of ImageJ. Specifically the plugin 3D Viewer was used for the 3D reconstruction.